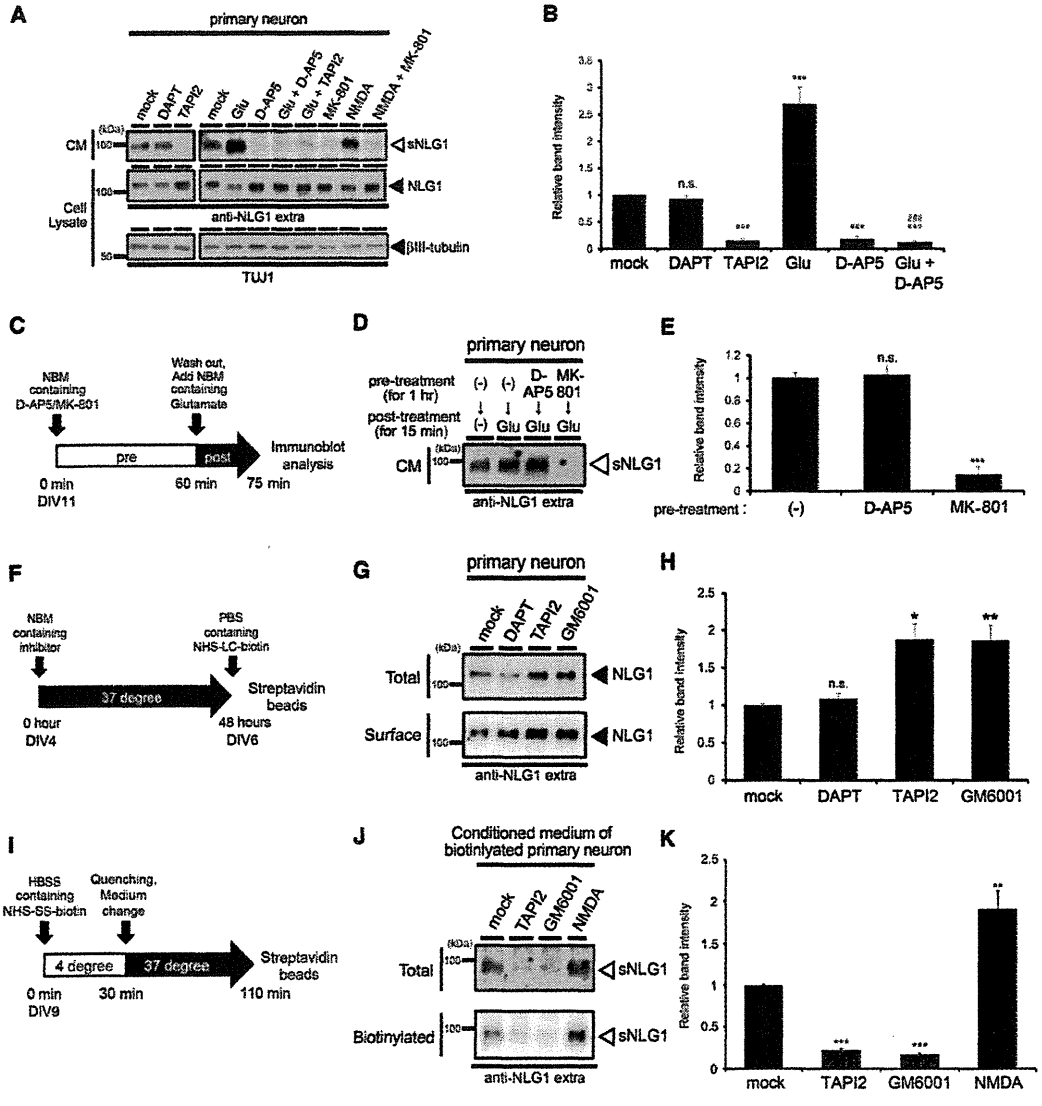

Figure 5. Activity-Dependent Shedding of NLG1 in Primary Neurons

(A) Primary neurons from E18 rat cortex were treated with indicated compounds at DIV11 for 15 min. CM as well as cell lysates were analyzed by immunoblotting using antibodies indicated below the panels.

(B) Densitometric analysis of the amounts of sNLG1 secreted from rat primary neurons treated as in (A). Statistical analysis was carried out by Student's t test (n = 5–9, mean ± SEM, ***$p < 0.001$ versus mock; ###$p < 0.001$ versus Glu).

(C–E) Production of sNLG1 from rat primary neurons from E17–E18 pups pretreated with NMDAR antagonists at DIV11 (C). Representative result of immunoblot analysis of CM is shown in (D). Noncompetitive NMDAR antagonist, MK-801, totally abolished the production of sNLG1. NBM indicates Neurobasal medium. Densitometric analysis of sNLG1 is shown in (E) (n = 3, mean ± SEM; ***$p < 0.001$ versus (–) by Student's t test).

(F–H) Surface protein levels were examined by the surface biotinylation technique in rat primary neurons obtained from E17–E18 pups at DIV6 (F). Representative result of immunoblot analysis is shown in (G). TAPI2 or GM6001 treatment from DIV4 to DIV6 caused a significant accumulation of total as well as cell surface NLG1. Densitometric analysis of sNLG1 is shown in (H) (n = 4, mean ± SEM; *$p < 0.05$; **$p < 0.01$ versus by Student's t test).

(I–K) Detection of de novo secretion of biotinylated sNLG1 from DIV9 rat primary neurons from E17–E18 pups (I). Representative result of immunoblot analysis is shown in (J). Densitometric analysis of sNLG1 is shown in (K) (n = 3–5, mean ± SEM; **$p < 0.01$; ***$p < 0.001$ versus mock by Student's t test).

a cell surface biotinylation experiment in rat primary neurons (Figure 5F). Treatment with TAPI2 or GM6001 significantly increased the surface levels of NLG1 (Figures 5G and 5H). Moreover, secretion of biotinylated sNLG1 was detected in the conditioned media of labeled primary neurons (Figures 5I, 5J, and 5K). Notably, increased sNLG1 by NMDA treatment also was biotinylated, suggesting that the proteolytic processing of NLG1 occurs at the cell surface and regulates the levels of cell surface

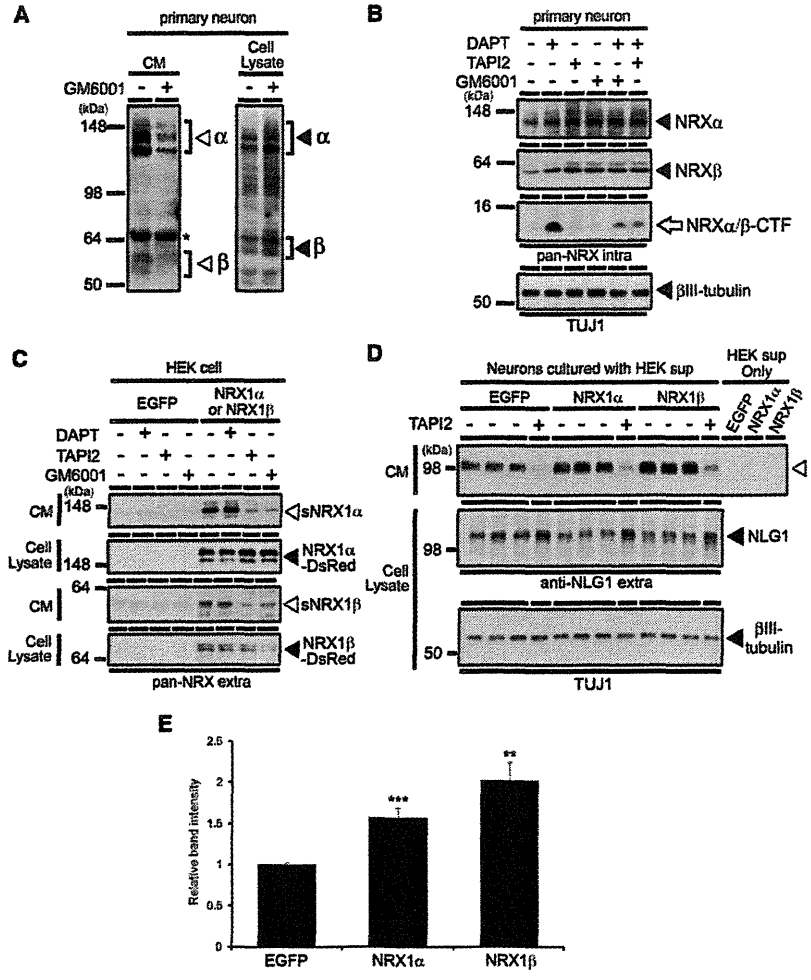

Figure 6. Increased Shedding of NLG1 by Soluble NRXs Derived by Proteolytic Processing

(A and B) Immunoblot analysis of serum-free CM as well as cell lysates of primary neurons with indicated compounds. Antibody against extracellular (A) or intracellular (B) domain of NRX was used.

(C) Metalloprotease-dependent secretion of recombinant soluble NRXs from HEK293T stably expressing NRX1α-dsRed or NRX1β-dsRed.

(D) DIV11 primary neurons from E18 rat were cultured for 24 hr in the presence of conditioned media derived from HEK293T stably expressing NRX1α or 1β, which was analyzed in (C). The levels of sNLG1 (white arrowhead) and NLG1-FL (black arrowhead) were analyzed by immunoblotting.

(E) Densitometric analysis of sNLG1 in (D) (n = 5–6, mean ± SEM; $^{**}p < 0.01$; $^{***}p < 0.001$ versus EGFP by Student's t test).

NLG1. Taken together with the results of synaptoneurosome incubation (Figure 1D), these data indicate that glutamatergic synaptic transmission through NMDA receptor activation modulates the levels of NLG1 at the synaptic membrane.

It has been shown that several γ-secretase substrates are cleaved upon binding with cognate membrane-tethered or soluble ligands, e.g., Delta/Jagged for Notch (Mumm et al., 2000), Hyaluronan for CD44 (Sugahara et al., 2003), BDNF for p75 (Kenchappa et al., 2006), and VEGF-A for VEGF receptor (Swendeman et al., 2008). Recently, it was reported that NRXs undergo proteolytic processing, which is augmented by glutamate treatment (Bot et al., 2011; Saura et al., 2011). We also observed the metalloprotease-dependent production of soluble forms of endogenous NRXs in rat primary neurons (Figure 6A). Treatment with TAPI2 or GM6001 caused the accumulation of NRX-FL and inhibited the accumulation of NRX-CTF, which was detected upon DAPT treatment (Figure 6B). These data indicate that NRXs also are sequentially cleaved by metalloprotease and γ-secretase in primary neurons. To investigate whether the binding of NRX regulates the production of sNLG1, we coincubated primary neurons with the conditioned media of HEK293T cells expressing NRX1α or NRX1β, which contained soluble forms of the NRXs (Figure 6C). Accumulation of NRX1β immunoreactivity at endogenous NLG1 puncta was observed in rat primary neurons treated with the HEK293T conditioned media containing sNRX1β, suggesting that recombinant sNRX1β is capable of interacting with NLG1 at synapses (Figure S4). Intriguingly, release of sNLG1 from neurons was significantly increased by addition of the soluble NRX-containing media (Figures 6D and 6E). This result indicates that ligand binding at the cell surface regulates the shedding of NLG1.

We also analyzed the activity-dependent NLG1 processing in vivo. Pilocarpine treatment induces glutamate-mediated synaptic activation, resulting in status epilepticus associated with synapse remodeling (Isokawa, 1998; Kurz et al., 2008). In agreement with the previous reports (Kamenetz et al., 2003), APP processing was promoted in the brains of 8-week-old epileptic mice (Figure 7A). Moreover, the level of sNLG1 was significantly increased, whereas that of the membrane-associated NLG1-FL was decreased, suggesting that NLG1 shedding was augmented in brains by pilocarpine-induced seizures (Figure 7B). Taken together, these data suggest that NLG1 processing is modulated by the excitatory activity in vivo as well as in vitro.

The Effect of NLG1 Processing on the Spine Density

To analyze the functional impact of NLG1 processing on its spinogenic activity, we overexpressed NLG1 and its derivatives in dentate granule cells of the organotypic hippocampal slice culture obtained from P6 rat, in which local-circuit synaptic interactions are preserved. Overexpression of NLG1-FL significantly increased the spine density at the apical dendrites of granule cells. However, NLG2-FL failed to induce spines, suggesting that NLG1 specifically increased the spine density at

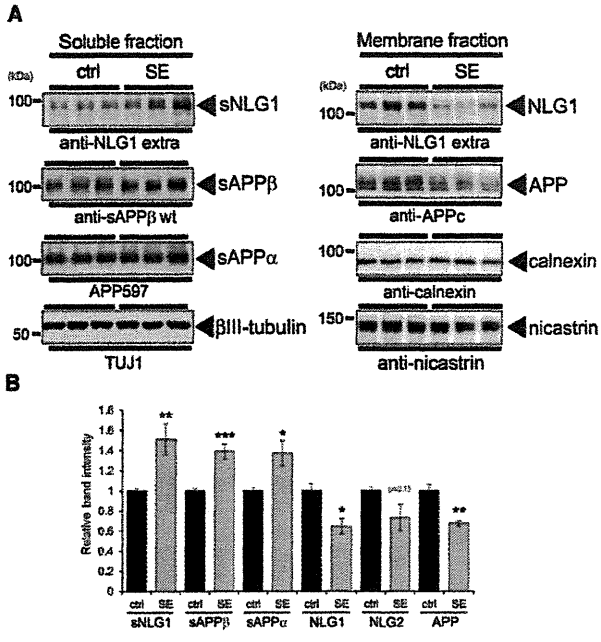

Figure 7. Status Epilepticus Induced by Pilocarpine Promoted the Shedding of NLG1 In Vivo

(A) Immunoblot analysis of TS soluble (soluble fraction, left) and insoluble (membrane fraction, right) of cortices from 8-week-old mice with status epilepticus (SE) 1 hr after the injection of pilocarpine. Mice injected with saline were used as control (ctrl). NLG1, APP, and their derivatives were probed with relevant antibodies. βIII-tubulin, calnexin, and nicastrin were used as loading controls for each fraction, respectively. A representative set of immunoblot data is shown.

(B) Densitometric analysis of immunoblots. Protein levels in SE brain were standardized by those in the control brains. Statistical analysis was carried out by Student's t test (n = 5, mean ± SEM, $^{*}p < 0.05$; $^{**}p < 0.01$, $^{***}p < 0.001$ versus ctrl).

glutamatergic synapses as previously described (Figure 8A) (Scheiffele et al., 2000; Graf et al., 2004). Overexpression of NLG1ΔPDZ that lacks the C terminus failed to increase the spine number, suggesting that the spinogenic effect of NLG1 is dependent on the PDZ-binding motif in rat dentate granule cells. Reduction in the amount of transfected NLG1 cDNA led to loss of the spinogenic effect of NLG1 (see 0.1 μg HA-NLG1, Figures 8A and 8B), indicating that the protein level of NLG1 is critical to the de novo formation of the dendritic spine (Figure 8B). Notably, TAPI2 treatment of cultures transfected with reduced amount of HA-NLG1 cDNA (0.1 μg/ml) recovered the incremental effect on spine density to a level comparable to that in cells transfected with 1.0 μg/μl of HA-NLG1. Thus, we reasoned that ectodomain shedding negatively regulates the spinogenic effect of NLG1 in hippocampal granule cells. Next, we analyzed the effects of fragment forms of NLG1 corresponding to its proteolytic products (i.e., NLG1-ΔE and NLG1-ICD) on the spine density (Figure 8A). Unexpectedly, NLG1-ΔE increased the spine density at a similar level to NLG1-FL, suggesting that the NLG1-CTF lacking the ectodomain retains the spinogenic effect. However, NLG1-ICD failed to increase the spine density. Thus, the function of membrane-tethered form of NLG1-ICD (aka,

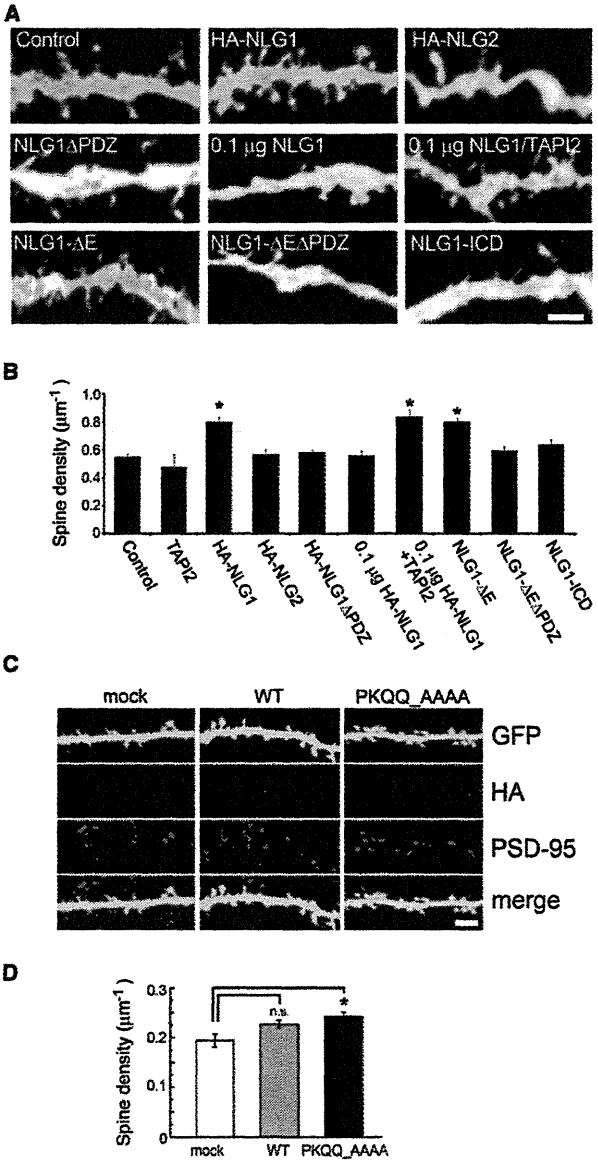

Figure 8. Effect of Truncated NLG1 on Spine Formation

(A) Representative confocal images of apical dendrites visualized by GFP in rat hippocampal slice cultures prepared from P6 rats transfected with GFP with NLG1 constructs. We used 1 μg of plasmids for recombinant proteins unless the amount is indicated. White bar represents 1 μm.

(B) Quantification of the spine density of neurons in the indicated conditions. Statistical analysis was carried out by Dunnett's multiple comparison test (n = 6–35, mean ± SEM, $^{*}p < 0.01$ versus mock).

(C) Representative confocal images of immunostained dendrites in rat hippocampal primary neurons obtained from E17–E18 pups transfected with GFP and WT or PKQQ_AAAA mutant NLG1. Transfection into rat primary neurons was performed at DIV6 and fixed at DIV20. White bar represents 5 μm.

(D) Quantification of the spine density of neurons under the indicated conditions. Statistical analysis was carried out by Dunnett's multiple comparison test (n = 14 [mock], 55 [WT], and 42 [PKQQ_AAAA]). Mean ± SEM, $^{*}p < 0.05$ versus mock.

NLG1-ΔE or NLG1-CTF) was abolished by liberation from the membrane by the γ-secretase cleavage and subsequent degradation. Finally, to directly test whether NLG1 shedding modulates the spinogenic function, we analyzed the dendritic spines of transfected rat hippocampal primary neurons obtained from E18 pups (Figure 8C). We transfected wild-type or PKQQ/AAAA mutant NLG1 together with green fluorescent protein (GFP) into primary neurons at DIV6 and fixed them at DIV20. The numbers of spines in neurons expressing wild-type NLG1 showed an increased trend compared to those in mock-transfected neurons, but not with a statistical significance. However, the spine density was significantly increased in neurons transfected with the mutant NLG1 (Figure 8D), suggesting that cleavage-deficient mutation enhanced the NLG1 function in primary neurons. Taken together, our results indicate that the sequential processing of NLG1 negatively regulates the spinogenic activity.

DISCUSSION

Sequential Proteolytic Processing of NLG1 by ADAM10 and γ-Secretase

To date, all known γ-secretase substrates are shown to be first shed at the extracellular domain to generate a soluble ectodomain as well as a membrane-tethered CTF. ADAM10 is a well-characterized physiological sheddase for a number of γ-secretase substrates (e.g., APP, cadherin, and Notch) (Reiss et al., 2005; Jorissen et al., 2010; Kuhn et al., 2010). Both γ-secretase and ADAM10 have been implicated in the regulation of neural stem cell number by modulation of Notch signaling in the developing CNS (Jorissen et al., 2010). Recently, it was shown that metalloprotease and γ-secretase-mediated cleavage in mature neurons regulates the synaptic function (Rivera et al., 2010; Restituito et al., 2011). Here we systematically analyzed the processing of NLG1 by pharmacological and genetic approaches. Using specific inhibitors and Cre-mediated gene excision, we found that ADAM10 is responsible for NLG1 shedding and that C-terminal stub of NLG1 is subsequently cleaved by γ-secretase (Figure 1F). Notably, significant reduction in the sNLG1 production was similarly observed in two distinct lines of *Adam10*$^{flox/flox}$ mice (i.e., exon 1 floxed mice for in vitro Cre-mediated gene excision in primary neurons and exon 2 floxed mice for cKO mice), indicating that ADAM10 is a major sheddase for NLG1 in vivo in brains. In addition, *Adam10*-dependent sNLG1 production and NLG1 accumulation were observed in primary neurons as well as in adult mouse brains, suggesting that NLG1 is shed by ADAM10 at both developmental and mature stages in neurons. Our data unequivocally indicate that the cell surface level of NLG1 is regulated by ADAM10/γ-secretase-mediated sequential processing, which may in turn negatively modulate its spinogenic activity.

It is noteworthy that ADAM10 prefers Leu, Phe, Tyr, and Gln at P1′ position for cleavage (Caescu et al., 2009), although no consensus cleavage sequence has been reported. Our observation that shedding of NLG1 was inhibited in PKQQ/AAAA mutant suggests that the Gln^{680} or Gln^{681} at the stalk region of NLG1 is the candidate cleavage site for ADAM10-mediated shedding. Unexpectedly, we found that NLG2 was not a suitable substrate for ADAMs so far examined. This is consistent with the previous results that ADAM10 is localized at the excitatory postsynapses at which NLG1 is present (Marcello et al., 2007), whereas NLG2 resides in the GABAergic postsynapses (Graf et al., 2004). Indeed, primary amino acid sequence of the stalk region of NLG2 is totally different from that of NLG1 (Figure 3A). Thus, other metalloprotease(s) present in the inhibitory synapse should be responsible for NLG2 shedding. Intriguingly, the expression levels of NLG1, but not NLG2, was significantly increased in the brains of ADAM10 transgenic mice, suggesting a specific functional correlation between NLG1 and ADAM10 (Prinzen et al., 2009). Identification of the responsible proteases and relevant auxiliary components at different types of synapses would provide important information on the proteolytic control of neuronal adhesion molecules.

Physiological Significance of the Activity-Dependent Processing of NLG1

The level of NLG1 in neurons has been shown to regulate the number, ratio of NMDA/AMPA receptors, and electrophysiological functions of the excitatory synapses in vitro and in vivo (Song et al., 1999; Chih et al., 2006; Varoqueaux et al., 2006; Chubykin et al., 2007). Here, we show that NLG1 is cleaved in a neuronal activity-dependent manner, resulting in a loss of its spinogenic function. Moreover, pretreatment with MK-801 completely abolished the processing of NLG1 induced by glutamate, suggesting that the NLG1 level is homeostatically controlled by the excitatory synaptic, but not extrasynaptic, transmission. Increased shedding of NLG1 was also observed in pilocarpine-treated mice. Interestingly, profound decreases in the density, as well as alterations in shape and size, of dendritic spines by aberrant Ca^{2+} signaling have been observed in epileptic mouse models (Isokawa, 1998; Kochan et al., 2000; Kurz, et al., 2008). Aberrant Ca^{2+} signaling also affects ADAM10 activity via calmodulin kinase as well as calcineurin (Nagano et al., 2004; Kohutek et al., 2009). These results support the idea that NLG1 processing is involved in the remodeling of dendritic spines at glutamatergic synapses in vivo. We also found that soluble NRX treatment augments the NLG1 shedding. In this regard, the activity-dependent proteolytic cleavage of NRX at the presynapse (Bot et al., 2011; Saura et al., 2011) may be functionally linked to the processing of NLG. It has been reported that Fc-fused recombinant NRX extracellular domain inhibited the synaptogenic activity of NLG (Scheiffele et al., 2000; Levinson et al., 2005); it is possible that soluble NRX functions as a negative regulator of NLG1 via induction of shedding. Ligand-induced shedding has been reported in several γ-secretase substrates (Mumm et al., 2000; Sugahara et al., 2003; Kenchappa et al., 2006; Findley et al., 2007) too, although the molecular mechanisms whereby the ligands activate the processing remain unknown. Ligand/receptor complex formation has been shown to increase the ADAM activity in the ephrin/Eph receptor system (Janes et al., 2009). In the case of Notch, "pulling" movement induced by the endocytosis of bound ligand is thought to cause a structural change leading to cleavage (Gordon et al., 2007). Notably, mucin-like *O*-linked glycosylation, which might create steric hindrance against ADAM10, was identified in the juxtamembranous stalk region of NLG1 (i.e., Ser^{683} and Ser^{686}, respectively; Hoffman et al., 2004). We also have found that

amino acid substitutions including the O-glycosylation sites (i.e., PSPF/AAAA and SVDQ/AAAA mutants) increased the shedding of NLG1 (Figure 4C). Thus, it is possible that the binding of soluble NRX induces structural changes in the stalk region of NLG1 in a way to expose the cleavage site and/or activate the ADAM10 activity. Further studies on the mechanism of ADAM10 activation as well as structural analyses of the cleavage site would clarify the mechanism of NLG1 shedding.

What, then, is the physiological function of the NLG1 fragments? Extracellular domain of NLG1 is sufficient for binding its ligands (Ichtchenko et al., 1995). Intriguingly, soluble form of NLG1 has been shown to inhibit the synaptogenic effect of TSP1 in immature neurons (Xu et al., 2010). Moreover, clustering of NRXs by recombinant NLG1 extracellular domain mediated the assembly of presynaptic terminals (Dean et al., 2003), raising the possibility that sNLG1 may bind to soluble as well as membrane-tethered forms of ligands and modulate their functions. Unexpectedly, however, overexpression of NLG1-ΔE that lacks the extracellular domain retained the capacity to induce dendritic spines in granule cells. Our observation is consistent with the previous data showing that the conserved cytoplasmic domain, rather than NRX binding, is necessary and sufficient for the induction of dendritic spines by NLG1 in transfected neurons (Ko et al., 2009; Shipman et al., 2011). Importantly, however, overexpression of NLG1-ICD, which retains the intact intracellular domain, failed to increase the spine numbers. Moreover, NLG1-ICD was highly labile and degraded by proteasomal activity. These data indicate that the membrane tethering as well as the stability of the cytoplasmic domain of NLG1 is critical to the spinogenic activity. This is distinct from the activation of the "conventional" γ-secretase substrates, e.g., Notch, by γ-cleavage, although there also are several examples of negative regulation of the functions of γ-secretase substrates by cleavage, e.g., ephrin-B1 and DCC (Tomita et al., 2006; Parent et al., 2005).

Taken together, our present results provide compelling evidence that proteolytic processing is a molecular mechanism regulating the NLG1 levels as well as its spinogenic function. Further functional analysis would be required to determine whether spines modulated by NLG1 shedding are functional. However, previous results showing that changes in spines by overexpression or knockdown of NLG1 correlated with synaptic transmission (Chih et al., 2006; Levinson et al., 2005; Chubykin et al., 2007) may support our view that the proteolytic cleavage by ADAM10 and γ-secretase downregulates the cell-surface levels of NLG1, which in turn negatively affects the synaptogenic function. Considering the recent implication of aberrant levels of expression of NLGs or NRXs in ASD, it is tempting to speculate that alterations in the proteolytic processing of NLG1 may also be involved in the etiology of the neurodevelopmental abnormalities.

EXPERIMENTAL PROCEDURES

Chemicals, Immunological Methods, Animals, Plasmids, Cell Culture, Transfection, Recombinant Virus Infection, and RNA Interference

All experimental procedures were performed in accordance with the guidelines for animal experiments of the University of Tokyo. Primary neuron culture, immunoblot analyses, and immunocytochemistry experiments were performed as previously described with some modifications (Tomita et al., 1998; Fukumoto et al., 1999). For in vitro Cre-mediated *Adam10* ablation, primary cortical neurons were obtained from E16 pups of *Adam10*$^{flox/flox}$ mice, in which the first exon was floxed (Yoda et al., 2011). For analysis of neuron-specific conditional *Adam10* knockout mice, brains of P18 exon 2 floxed *Adam10*$^{flox/flox}$ mice (Jorissen et al., 2010) crossed with CamKII-Cre mice (J.P. and P.S., unpublished data) were homogenized to obtain microsome fractions. Other animals were obtained from Japan-SLC. See Supplemental Experimental Procedures for details.

Mouse Model of Status Epilepticus by Pilocarpine Treatment

Male 8-week-old BALB/C mice were injected with scopolamine methylnitrate (Tokyo Chemical Industry) (1 mg/kg, intraperitoneally [i.p.]) to protect against peripheral autonomic effects caused by subsequent pilocarpine administration. Fifteen to thirty minutes later, mice were injected with pilocarpine-HCl (SIGMA) (330–380 mg/kg, i.p.) or saline (Otsuka), and then we scored the seizure intensity according to a previously described method (Patel et al., 1988). We defined status epilepticus (status epilepsy) as a continuous seizure lasting longer than 30 min. One hour after the injection of pilocarpine, mice were sacrificed to isolate the cerebrums. See Supplemental Experimental Procedures for details.

Analysis of Spinogenic Function of NLG1

Hippocampal slice cultures were prepared from P6 rats as previously described (Koyama et al., 2007). Granule cells in the cultured slices at DIV5 were transfected with the plasmids encoding NLG1 and its derivatives (1.0 μg/μl in HBSS) using the single-cell electroporation method (Nakahara et al., 2009). Transfection of mutant NLG1 in rat hippocampal primary neurons were performed at DIV6 and fixed at DIV20. See Supplemental Experimental Proceduresfor details.

SUPPLEMENTAL INFORMATION

Supplemental Information includes four figures and Supplemental Experimental Procedures and can be found with this article online at http://dx.doi.org/10.1016/j.neuron.2012.10.003.

ACKNOWLEDGMENTS

We thank Drs. C. Blobel (Hospital for Special Surgery, New York), R. Balice-Gordon (University of Pennsylvania), P. Scheiffele (University of Basel), B. De Strooper (VIB Leuven), K. Hozumi (Tokai University), F. Fahrenholtz (Johannes Gutenberg University Mainz), T. Kitamura (The University of Tokyo), and J. Takagi (Osaka University) for materials. We are also grateful to our laboratory members for helpful discussions and technical assistance. This work was supported by Grants-in-Aid for Young Scientists (S) from Japan Society for the Promotion of Science (JSPS) (for T.T.), Challenging Exploratory Research from JSPS (for T.T.), Scientific Research on Innovative Areas "Foundation of Synapse and Neurocircuit Pathology" from the Ministry of Education, Culture, Sports, Science, and Technology (MEXT) (for T.T. and T.I.), the Cell Science Research Foundation (for T.T.), Core Research for Evolutional Science and Technology of the Japan Science and Technology Agency (for Y.H., T.T., and T.I.), Japan, and the Deutsche Forschungsgemeinschaft SFB877 TP:A3 (for P.S.). K.S. is a research fellow of JSPS.

Accepted: October 2, 2012
Published: October 18, 2012

REFERENCES

Bai, G., and Pfaff, S.L. (2011). Protease regulation: the Yin and Yang of neural development and disease. Neuron *72*, 9–21.

Beel, A.J., and Sanders, C.R. (2008). Substrate specificity of γ-secretase and other intramembrane proteases. Cell. Mol. Life Sci. *65*, 1311–1334.

Blundell, J., Blaiss, C.A., Etherton, M.R., Espinosa, F., Tabuchi, K., Walz, C., Bolliger, M.F., Südhof, T.C., and Powell, C.M. (2010). Neuroligin-1 deletion

results in impaired spatial memory and increased repetitive behavior. J. Neurosci. *30*, 2115–2129.

Bot, N., Schweizer, C., Ben Halima, S., and Fraering, P.C. (2011). Processing of the synaptic cell adhesion molecule neurexin-3β by Alzheimer disease α- and γ-secretases. J. Biol. Chem. *286*, 2762–2773.

Bottos, A., Rissone, A., Bussolino, F., and Arese, M. (2011). Neurexins and neuroligins: synapses look out of the nervous system. Cell. Mol. Life Sci. *68*, 2655–2666.

Budreck, E.C., and Scheiffele, P. (2007). Neuroligin-3 is a neuronal adhesion protein at GABAergic and glutamatergic synapses. Eur. J. Neurosci. *26*, 1738–1748.

Caescu, C.I., Jeschke, G.R., and Turk, B.E. (2009). Active-site determinants of substrate recognition by the metalloproteinases TACE and ADAM10. Biochem. J. *424*, 79–88.

Chih, B., Gollan, L., and Scheiffele, P. (2006). Alternative splicing controls selective trans-synaptic interactions of the neuroligin-neurexin complex. Neuron *51*, 171–178.

Chubykin, A.A., Atasoy, D., Etherton, M.R., Brose, N., Kavalali, E.T., Gibson, J.R., and Südhof, T.C. (2007). Activity-dependent validation of excitatory versus inhibitory synapses by neuroligin-1 versus neuroligin-2. Neuron *54*, 919–931.

Comoletti, D., De Jaco, A., Jennings, L.L., Flynn, R.E., Gaietta, G., Tsigelny, I., Ellisman, M.H., and Taylor, P. (2004). The Arg451Cys-neuroligin-3 mutation associated with autism reveals a defect in protein processing. J. Neurosci. *24*, 4889–4893.

Dahlhaus, R., Hines, R.M., Eadie, B.D., Kannangara, T.S., Hines, D.J., Brown, C.E., Christie, B.R., and El-Husseini, A. (2010). Overexpression of the cell adhesion protein neuroligin-1 induces learning deficits and impairs synaptic plasticity by altering the ratio of excitation to inhibition in the hippocampus. Hippocampus *20*, 305–322.

Dalva, M.B., McClelland, A.C., and Kayser, M.S. (2007). Cell adhesion molecules: signalling functions at the synapse. Nat. Rev. Neurosci. *8*, 206–220.

Dean, C., Scholl, F.G., Choih, J., DeMaria, S., Berger, J., Isacoff, E., and Scheiffele, P. (2003). Neurexin mediates the assembly of presynaptic terminals. Nat. Neurosci. *6*, 708–716.

Findley, C.M., Cudmore, M.J., Ahmed, A., and Kontos, C.D. (2007). VEGF induces Tie2 shedding via a phosphoinositide 3-kinase/Akt dependent pathway to modulate Tie2 signaling. Arterioscler. Thromb. Vasc. Biol. *27*, 2619–2626.

Fukumoto, H., Tomita, T., Matsunaga, H., Ishibashi, Y., Saido, T.C., and Iwatsubo, T. (1999). Primary cultures of neuronal and non-neuronal rat brain cells secrete similar proportions of amyloid β peptides ending at Aβ40 and Aβ42. Neuroreport *10*, 2965–2969.

Glessner, J.T., Wang, K., Cai, G., Korvatska, O., Kim, C.E., Wood, S., Zhang, H., Estes, A., Brune, C.W., Bradfield, J.P., et al. (2009). Autism genome-wide copy number variation reveals ubiquitin and neuronal genes. Nature *459*, 569–573.

Gordon, W.R., Vardar-Ulu, D., Histen, G., Sanchez-Irizarry, C., Aster, J.C., and Blacklow, S.C. (2007). Structural basis for autoinhibition of Notch. Nat. Struct. Mol. Biol. *14*, 295–300.

Graf, E.R., Zhang, X., Jin, S.X., Linhoff, M.W., and Craig, A.M. (2004). Neurexins induce differentiation of GABA and glutamate postsynaptic specializations via neuroligins. Cell *119*, 1013–1026.

Hartmann, D., de Strooper, B., Serneels, L., Craessaerts, K., Herreman, A., Annaert, W., Umans, L., Lübke, T., Lena Illert, A., von Figura, K., and Saftig, P. (2002). The disintegrin/metalloprotease ADAM 10 is essential for Notch signalling but not for α-secretase activity in fibroblasts. Hum. Mol. Genet. *11*, 2615–2624.

Herreman, A., Serneels, L., Annaert, W., Collen, D., Schoonjans, L., and De Strooper, B. (2000). Total inactivation of γ-secretase activity in presenilin-deficient embryonic stem cells. Nat. Cell Biol. *2*, 461–462.

Hoffman, R.C., Jennings, L.L., Tsigelny, I., Comoletti, D., Flynn, R.E., Sudhof, T.C., and Taylor, P. (2004). Structural characterization of recombinant soluble rat neuroligin 1: mapping of secondary structure and glycosylation by mass spectrometry. Biochemistry *43*, 1496–1506.

Horiuchi, K., Miyamoto, T., Takaishi, H., Hakozaki, A., Kosaki, N., Miyauchi, Y., Furukawa, M., Takito, J., Kaneko, H., Matsuzaki, K., et al. (2007). Cell surface colony-stimulating factor 1 can be cleaved by TNF-α converting enzyme or endocytosed in a clathrin-dependent manner. J. Immunol. *179*, 6715–6724.

Huettner, J.E., and Bean, B.P. (1988). Block of N-methyl-D-aspartate-activated current by the anticonvulsant MK-801: selective binding to open channels. Proc. Natl. Acad. Sci. USA *85*, 1307–1311.

Ichtchenko, K., Hata, Y., Nguyen, T., Ullrich, B., Missler, M., Moomaw, C., and Südhof, T.C. (1995). Neuroligin 1: a splice site-specific ligand for β-neurexins. Cell *81*, 435–443.

Inoue, E., Deguchi-Tawarada, M., Togawa, A., Matsui, C., Arita, K., Katahira-Tayama, S., Sato, T., Yamauchi, E., Oda, Y., and Takai, Y. (2009). Synaptic activity prompts γ-secretase-mediated cleavage of EphA4 and dendritic spine formation. J. Cell Biol. *185*, 551–564.

Irie, M., Hata, Y., Takeuchi, M., Ichtchenko, K., Toyoda, A., Hirao, K., Takai, Y., Rosahl, T.W., and Südhof, T.C. (1997). Binding of neuroligins to PSD-95. Science *277*, 1511–1515.

Isokawa, M. (1998). Remodeling dendritic spines in the rat pilocarpine model of temporal lobe epilepsy. Neurosci. Lett. *258*, 73–76.

Janes, P.W., Wimmer-Kleikamp, S.H., Frangakis, A.S., Treble, K., Griesshaber, B., Sabet, O., Grabenbauer, M., Ting, A.Y., Saftig, P., Bastiaens, P.I., and Lackmann, M. (2009). Cytoplasmic relaxation of active Eph controls ephrin shedding by ADAM10. PLoS Biol. *7*, e1000215.

Jorissen, E., Prox, J., Bernreuther, C., Weber, S., Schwanbeck, R., Serneels, L., Snellinx, A., Craessaerts, K., Thathiah, A., Tesseur, I., et al. (2010). The disintegrin/metalloproteinase ADAM10 is essential for the establishment of the brain cortex. J. Neurosci. *30*, 4833–4844.

Kamenetz, F., Tomita, T., Hsieh, H., Seabrook, G., Borchelt, D., Iwatsubo, T., Sisodia, S., and Malinow, R. (2003). APP processing and synaptic function. Neuron *37*, 925–937.

Kawaguchi, N., Horiuchi, K., Becherer, J.D., Toyama, Y., Besmer, P., and Blobel, C.P. (2007). Different ADAMs have distinct influences on Kit ligand processing: phorbol-ester-stimulated ectodomain shedding of Kitl1 by ADAM17 is reduced by ADAM19. J. Cell Sci. *120*, 943–952.

Kenchappa, R.S., Zampieri, N., Chao, M.V., Barker, P.A., Teng, H.K., Hempstead, B.L., and Carter, B.D. (2006). Ligand-dependent cleavage of the P75 neurotrophin receptor is necessary for NRIF nuclear translocation and apoptosis in sympathetic neurons. Neuron *50*, 219–232.

Kim, S.H., Fraser, P.E., Westaway, D., St George-Hyslop, P.H., Ehrlich, M.E., and Gandy, S. (2010). Group II metabotropic glutamate receptor stimulation triggers production and release of Alzheimer's amyloid(β)42 from isolated intact nerve terminals. J. Neurosci. *30*, 3870–3875.

Ko, J., Zhang, C., Arac, D., Boucard, A.A., Brunger, A.T., and Südhof, T.C. (2009). Neuroligin-1 performs neurexin-dependent and neurexin-independent functions in synapse validation. EMBO J. *28*, 3244–3255.

Kochan, L.D., Churn, S.B., Omojokun, O., Rice, A., and DeLorenzo, R.J. (2000). Status epilepticus results in an N-methyl-D-aspartate receptor-dependent inhibition of Ca2+/calmodulin-dependent kinase II activity in the rat. Neuroscience *95*, 735–743.

Kohutek, Z.A., diPierro, C.G., Redpath, G.T., and Hussaini, I.M. (2009). ADAM-10-mediated N-cadherin cleavage is protein kinase C-α dependent and promotes glioblastoma cell migration. J. Neurosci. *29*, 4605–4615.

Koyama, R., Muramatsu, R., Sasaki, T., Kimura, R., Ueyama, C., Tamura, M., Tamura, N., Ichikawa, J., Takahashi, N., Usami, A., et al. (2007). A low-cost method for brain slice cultures. J. Pharmacol. Sci. *104*, 191–194.

Kuhn, P.H., Wang, H., Dislich, B., Colombo, A., Zeitschel, U., Ellwart, J.W., Kremmer, E., Rossner, S., and Lichtenthaler, S.F. (2010). ADAM10 is the physiologically relevant, constitutive α-secretase of the amyloid precursor protein in primary neurons. EMBO J. *29*, 3020–3032.

Kurz, J.E., Moore, B.J., Henderson, S.C., Campbell, J.N., and Churn, S.B. (2008). A cellular mechanism for dendritic spine loss in the pilocarpine model of status epilepticus. Epilepsia *49*, 1696–1710.

Levinson, J.N., and El-Husseini, A. (2007). A crystal-clear interaction: relating neuroligin/neurexin complex structure to function at the synapse. Neuron *56*, 937–939.

Levinson, J.N., Chéry, N., Huang, K., Wong, T.P., Gerrow, K., Kang, R., Prange, O., Wang, Y.T., and El-Husseini, A. (2005). Neuroligins mediate excitatory and inhibitory synapse formation: involvement of PSD-95 and neurexin-1β in neuroligin-induced synaptic specificity. J. Biol. Chem. *280*, 17312–17319.

Marambaud, P., Wen, P.H., Dutt, A., Shioi, J., Takashima, A., Siman, R., and Robakis, N.K. (2003). A CBP binding transcriptional repressor produced by the PS1/ε-cleavage of N-cadherin is inhibited by PS1 FAD mutations. Cell *114*, 635–645.

Marcello, E., Gardoni, F., Mauceri, D., Romorini, S., Jeromin, A., Epis, R., Borroni, B., Cattabeni, F., Sala, C., Padovani, A., and Di Luca, M. (2007). Synapse-associated protein-97 mediates α-secretase ADAM10 trafficking and promotes its activity. J. Neurosci. *27*, 1682–1691.

Mumm, J.S., Schroeter, E.H., Saxena, M.T., Griesemer, A., Tian, X., Pan, D.J., Ray, W.J., and Kopan, R. (2000). A ligand-induced extracellular cleavage regulates γ-secretase-like proteolytic activation of Notch1. Mol. Cell *5*, 197–206.

Nagano, O., Murakami, D., Hartmann, D., De Strooper, B., Saftig, P., Iwatsubo, T., Nakajima, M., Shinohara, M., and Saya, H. (2004). Cell-matrix interaction via CD44 is independently regulated by different metalloproteinases activated in response to extracellular Ca(2+) influx and PKC activation. J. Cell Biol. *165*, 893–902.

Nakahara, S., Tamura, M., Matsuki, N., and Koyama, R. (2009). Neuronal hyperactivity sustains the basal dendrites of immature dentate granule cells: time-lapse confocal analysis using hippocampal slice cultures. Hippocampus *19*, 379–391.

Parent, A.T., Barnes, N.Y., Taniguchi, Y., Thinakaran, G., and Sisodia, S.S. (2005). Presenilin attenuates receptor-mediated signaling and synaptic function. J. Neurosci. *25*, 1540–1549.

Patel, S., Meldrum, B.S., and Fine, A. (1988). Susceptibility to pilocarpine-induced seizures in rats increases with age. Behav. Brain Res. *31*, 165–167.

Prinzen, C., Trümbach, D., Wurst, W., Endres, K., Postina, R., and Fahrenholz, F. (2009). Differential gene expression in ADAM10 and mutant ADAM10 transgenic mice. BMC Genomics *10*, 66.

Reiss, K., Maretzky, T., Ludwig, A., Tousseyn, T., de Strooper, B., Hartmann, D., and Saftig, P. (2005). ADAM10 cleavage of N-cadherin and regulation of cell-cell adhesion and β-catenin nuclear signalling. EMBO J. *24*, 742–752.

Restituito, S., Khatri, L., Ninan, I., Mathews, P.M., Liu, X., Weinberg, R.J., and Ziff, E.B. (2011). Synaptic autoregulation by metalloproteases and γ-secretase. J. Neurosci. *31*, 12083–12093.

Rivera, S., Khrestchatisky, M., Kaczmarek, L., Rosenberg, G.A., and Jaworski, D.M. (2010). Metzincin proteases and their inhibitors: foes or friends in nervous system physiology? J. Neurosci. *30*, 15337–15357.

Saftig, P., and Reiss, K. (2011). The "A Disintegrin And Metalloproteases" ADAM10 and ADAM17: novel drug targets with therapeutic potential? Eur. J. Cell Biol. *90*, 527–535.

Saura, C.A., Servián-Morilla, E., and Scholl, F.G. (2011). Presenilin/γ-secretase regulates neurexin processing at synapses. PLoS ONE *6*, e19430.

Schapitz, I.U., Behrend, B., Pechmann, Y., Lappe-Siefke, C., Kneussel, S.J., Wallace, K.E., Stempel, A.V., Buck, F., Grant, S.G., Schweizer, M., et al. (2010). Neuroligin 1 is dynamically exchanged at postsynaptic sites. J. Neurosci. *30*, 12733–12744.

Scheiffele, P., Fan, J., Choih, J., Fetter, R., and Serafini, T. (2000). Neuroligin expressed in nonneuronal cells triggers presynaptic development in contacting axons. Cell *101*, 657–669.

Shipman, S.L., Schnell, E., Hirai, T., Chen, B.S., Roche, K.W., and Nicoll, R.A. (2011). Functional dependence of neuroligin on a new non-PDZ intracellular domain. Nat. Neurosci. *14*, 718–726.

Siddiqui, T.J., and Craig, A.M. (2011). Synaptic organizing complexes. Curr. Opin. Neurobiol. *21*, 132–143.

Song, J.Y., Ichtchenko, K., Südhof, T.C., and Brose, N. (1999). Neuroligin 1 is a postsynaptic cell-adhesion molecule of excitatory synapses. Proc. Natl. Acad. Sci. USA *96*, 1100–1105.

Südhof, T.C. (2008). Neuroligins and neurexins link synaptic function to cognitive disease. Nature *455*, 903–911.

Sugahara, K.N., Murai, T., Nishinakamura, H., Kawashima, H., Saya, H., and Miyasaka, M. (2003). Hyaluronan oligosaccharides induce CD44 cleavage and promote cell migration in CD44-expressing tumor cells. J. Biol. Chem. *278*, 32259–32265.

Swendeman, S., Mendelson, K., Weskamp, G., Horiuchi, K., Deutsch, U., Scherle, P., Hooper, A., Rafii, S., and Blobel, C.P. (2008). VEGF-A stimulates ADAM17-dependent shedding of VEGFR2 and crosstalk between VEGFR2 and ERK signaling. Circ. Res. *103*, 916–918.

Thyagarajan, A., and Ting, A.Y. (2010). Imaging activity-dependent regulation of neurexin-neuroligin interactions using trans-synaptic enzymatic biotinylation. Cell *143*, 456–469.

Tomita, T., Tokuhiro, S., Hashimoto, T., Aiba, K., Saido, T.C., Maruyama, K., and Iwatsubo, T. (1998). Molecular dissection of domains in mutant presenilin 2 that mediate overproduction of amyloidogenic forms of amyloid β peptides. Inability of truncated forms of PS2 with familial Alzheimer's disease mutation to increase secretion of Aβ42. J. Biol. Chem. *273*, 21153–21160.

Tomita, T., Tanaka, S., Morohashi, Y., and Iwatsubo, T. (2006). Presenilin-dependent intramembrane cleavage of ephrin-B1. Mol. Neurodegener. *1*, 2.

Varoqueaux, F., Jamain, S., and Brose, N. (2004). Neuroligin 2 is exclusively localized to inhibitory synapses. Eur. J. Cell Biol. *83*, 449–456.

Varoqueaux, F., Aramuni, G., Rawson, R.L., Mohrmann, R., Missler, M., Gottmann, K., Zhang, W., Südhof, T.C., and Brose, N. (2006). Neuroligins determine synapse maturation and function. Neuron *51*, 741–754.

Villasana, L.E., Klann, E., and Tejada-Simon, M.V. (2006). Rapid isolation of synaptoneurosomes and postsynaptic densities from adult mouse hippocampus. J. Neurosci. Methods *158*, 30–36.

Weskamp, G., Ford, J.W., Sturgill, J., Martin, S., Docherty, A.J., Swendeman, S., Broadway, N., Hartmann, D., Saftig, P., Umland, S., et al. (2006). ADAM10 is a principal 'sheddase' of the low-affinity immunoglobulin E receptor CD23. Nat. Immunol. *7*, 1293–1298.

Witters, L., Scherle, P., Friedman, S., Fridman, J., Caulder, E., Newton, R., and Lipton, A. (2008). Synergistic inhibition with a dual epidermal growth factor receptor/HER-2/neu tyrosine kinase inhibitor and a disintegrin and metalloprotease inhibitor. Cancer Res. *68*, 7083–7089.

Xu, J., Xiao, N., and Xia, J. (2010). Thrombospondin 1 accelerates synaptogenesis in hippocampal neurons through neuroligin 1. Nat. Neurosci. *13*, 22–24.

Yoda, M., Kimura, T., Tohmonda, T., Uchikawa, S., Koba, T., Takito, J., Morioka, H., Matsumoto, M., Link, D.C., Chiba, K., et al. (2011). Dual functions of cell-autonomous and non-cell-autonomous ADAM10 activity in granulopoiesis. Blood *118*, 6939–6942.

Zhang, C., Milunsky, J.M., Newton, S., Ko, J., Zhao, G., Maher, T.A., Tager-Flusberg, H., Bolliger, M.F., Carter, A.S., Boucard, A.A., et al. (2009). A neuroligin-4 missense mutation associated with autism impairs neuroligin-4 folding and endoplasmic reticulum export. J. Neurosci. *29*, 10843–10854.

Zhou, H.M., Weskamp, G., Chesneau, V., Sahin, U., Vortkamp, A., Horiuchi, K., Chiusaroli, R., Hahn, R., Wilkes, D., Fisher, P., et al. (2004). Essential role for ADAM19 in cardiovascular morphogenesis. Mol. Cell. Biol. *24*, 96–104.

Zhou, B.B., Peyton, M., He, B., Liu, C., Girard, L., Caudler, E., Lo, Y., Baribaud, F., Mikami, I., Reguart, N., et al. (2006). Targeting ADAM-mediated ligand cleavage to inhibit HER3 and EGFR pathways in non-small cell lung cancer. Cancer Cell *10*, 39–50.

BIOCHEMISTRY
including biophysical chemistry & molecular biology

Article

pubs.acs.org/biochemistry

Inhibition of γ-Secretase Activity by a Monoclonal Antibody against the Extracellular Hydrophilic Loop of Presenilin 1

Shizuka Takagi-Niidome,[†] Satoko Osawa,[†] Taisuke Tomita,*[,†,‡] and Takeshi Iwatsubo[†,‡,§]

[†]Department of Neuropathology and Neuroscience, Graduate School of Pharmaceutical Sciences, The University of Tokyo, Tokyo 113-0033, Japan

[‡]Core Research for Evolutional Science and Technology, Japan Science and Technology Agency, Tokyo 113-0033, Japan

[§]Department of Neuropathology, Graduate School of Medicine, The University of Tokyo, Tokyo 113-0033, Japan

ABSTRACT: Presenilin 1 (PS1) comprises a catalytic subunit of γ-secretase, which is an intramembrane-cleaving protease responsible for generation of amyloid-β peptides as well as Notch cleavage, the latter being implicated in cancer. We have shown that transmembrane domains (TMDs) 1, 6, 7, and 9 of PS1 form the "catalytic pore" structure within the membrane for intramembrane proteolysis. Here we report a novel monoclonal antibody 9D11, which directly recognizes the TMD1-proximal residues in the hydrophilic loop region. Intriguingly, 9D11 inhibited the γ-secretase activity irrespective of the binding of known γ-secretase inhibitors and abolished Notch signaling-dependent cancer cell viability. Our data suggest that the juxtamembrane region of TMD1 of PS1 is a novel molecular target for the mechanism-based inhibition of γ-secretase and the development of the anticancer drug.

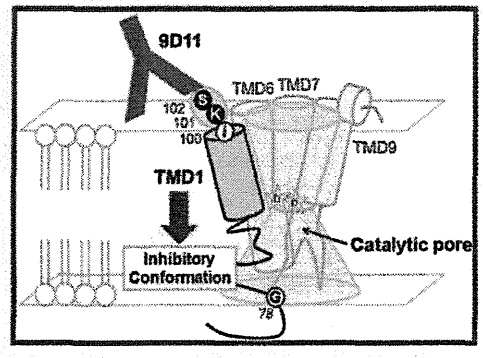

Intramembrane proteolysis is an atypical hydrolysis of peptide bonds within the lipid bilayer. Several lines of evidence suggest that this atypical cleavage is involved in numerous biological processes encompassing all branches of life. So far, four families of intramembrane-cleaving proteases have been discovered: rhomboid, site-2 protease (S2P), signal peptide peptidase, and γ-secretase.[1] γ-Secretase is a key enzyme in the production of amyloid-β peptide (Aβ), a major component of senile plaques in the brains of patients with Alzheimer's disease.[2,3] Moreover, γ-secretase mediates proteolysis-dependent signaling of several type I membrane proteins, including the Notch receptor, which is involved in the development of cancer.[3,4] Thus, rational design of γ-secretase inhibitors (GSIs) based on the molecular mechanism of γ-secretase would pave the way for the development of novel drugs.[5] However, structural analysis of γ-secretase has not been fully achieved; this atypical protease is comprised of at least four transmembrane proteins: nicastrin (Nct), anterior pharynx defective-1 (Aph-1), presenilin enhancer-2 (Pen-2), and PS1, the latter representing the catalytic subunit.[3,6] In contrast, structural analyses of rhomboid and S2P family intramembrane proteases have revealed that membrane-embedded active sites of these proteases are indeed hydrated within the intramembrane cavity or channel-like structure.[7] These data suggest that hydrolysis of transmembrane helices occurs within the membrane. However, the molecular and structural bases of the recognition and incorporation of the hydrophobic substrates remain unknown.

We have been applying the substituted cysteine accessibility method (SCAM) to gain insight into the structure of PS1 in a membrane-embedded state. The SCAM has been reiteratively used to obtain structural information about various multipass membrane proteins in a functional state, by covalently modifying the introduced cysteine (Cys) residues using sulfhydryl reagents.[8−10] Using the SCAM, we and others have revealed that PS1 harbors a hydrophilic "catalytic pore" formed by TMD1, -6, -7, and -9.[11−15] This suggests that the hydrophilic milieu around the active site located within the lipid bilayer is a common structure across intramembrane-cleaving proteases. In addition, upon incubation of GSI, we identified the movement of TMD1 of PS1 [i.e., from glycine 78 (G78) to isoleucine 100 (I100)] downward to the cytosolic side, which was evidenced by specific changes in the hydrophilicity of the microenvironment of amino acid residues located at the borders of TMD1 (i.e., G78 and I100) in the SCAM.[15] Here we developed rat monoclonal antibody (mAb) 9D11 against the juxtamembrane region of TMD1. Intriguingly, 9D11 treatment reduced the γ-secretase activity as well as the extent of growth of the cancer cell line. However, a photoaffinity labeling experiment revealed that the binding mode of 9D11 is totally distinct from that of the small compound-based known GSIs. Our data indicate that the juxtamembrane region of TMD1 might be a novel target domain for the development of therapeutics against cancer caused by an abnormal upregulation of γ-secretase activity.[3,4]

Received: September 13, 2012
Revised: December 4, 2012
Published: December 4, 2012

EXPERIMENTAL PROCEDURES

Production and Purification of Anti-Hydrophilic Loop 1 of PS1 mAbs. All experimental procedures were performed in accordance with the guidelines for animal experiments of The University of Tokyo. Glutathione *S*-transferase (GST) fusion protein containing residues K101−M139 of PS1 [GST hydrophilic loop 1 (HL1)] was purified using glutathione Sepharose 4B (GE Healthcare). Eight-week-old WKY/Izm rats were purchased from Japan SLC and immunized with 100 μg of purified GST-HL1 in Freund's complete adjuvant (Sigma), via footpad injection.[16] One month after the first boost, immunized rats were tail bled and serum titers were checked using an enzyme-linked immunosorbent assay (ELISA) (see below) and reboosted. B cells obtained from the iliac and inguinal lymph nodes were fused with a PAI myeloma cell that was a kind gift of H. Arai (The University of Tokyo). The hybridoma cells were cultured in HAT selection medium [GIT medium (Wako Pure Chemical Industries) containing 5% FBS (Hyclone), 5% NCTC109 (Invitrogen), 1% nonessential amino acids (Invitrogen), 1% penicillin-streptomycin-glutamine (Invitrogen), purified interleukin-6, 100 μM hypoxanthine, 0.4 μM aminopterin, and 16 μM thymidine]. The hybridoma supernatants were screened for antibodies using an ELISA with a KLH-conjugated synthetic peptide encoding K101−T124 of PS1 (BEX, Co. Ltd.). For the purification of mAbs, hybridoma cells were cultured in GIT medium containing 5% NCTC109, 1% nonessential amino acids, and 1% penicillin-streptomycin-glutamine. mAbs in cultured media were purified using the MAbTrap Kit (GE Healthcare) according to the manufacturer's instructions. Rat IgG used as the control IgG was purchased from Sigma-Aldrich Japan. Purified mAb was stored at −80 °C before use.

ELISA System for mAb Screening and Epitope Mapping. KLH-conjugated peptides and sequential peptides for epitope mapping were purchased from BEX and Sigma-Aldrich Japan, respectively. Peptides (10 μg/mL) or GST fusion proteins (1 μg/mL) in PBS were added to a 96-well plate and incubated overnight at 4 °C. The coated plates were blocked with PBS containing 3% bovine serum albumin and 0.1% sodium azide. The hybridoma cell culture supernatant or purified mAb in PBS was added and the mixture incubated overnight at 4 °C. After the wells had been washed four times with PBS, anti-rat IgG coupled to horseradish peroxidase (GE Healthcare) was added at a dilution of 1:2000 and incubated at room temperature for 2 h. The wells were washed six times with PBS and detected with a TMB microwell peroxidase substrate system (Kirkegaard & Perry Laboratories Inc.), and the optical density at 450 nm was measured.

Plasmid Construction, Cell Culture, Transfection, and Retroviral Infection. For the generation of GST-HL1, cDNAs encoding HL1 of PS1 were inserted into pGEX-6P-1 (GE Healthcare). cDNAs encoding PS1 and Cys-less PS1 were inserted into pMXs-puro as previously described.[11,17] Mutant forms of PS1 were generated using a long polymerase chain reaction-based protocol. Construction of SC100 fused with the gal4 sequence (SC100-gal4) in pcDNA3.1/Hyg(+), EGFP in pcDNA3, UAS-luc in pGL3(r2.2), SPC99gvp-6myc in pMXs-puro, NΔE-6myc in pLPCX, UAS-firefly luciferase in pMXs-EGFPII, and TP1-renilla luciferase in pMXs-II was conducted as previously described.[17−19] Maintenance of *Psen1*$^{-/-}$/*Psen2*$^{-/-}$ double-knockout embryonic fibroblast (DKO), Plat-E, HEK293, HeLa, and A549 cells, retroviral infection, and generation of stable infectant pools were conducted as described previously.[11,12,15,17,19−22]

Antibodies, Immunochemical Analyses, and γ-Secretase Assays. Polyclonal antibodies G1Nr5, G1L3, and PNT3 against the N-terminus of PS1, the cytoplasmic loop region of PS1, and the N-terminal region of Pen-2, respectively, have been previously described.[18,23,24] C502 is a rabbit polyclonal antibody against recombinant protein encoding the C-terminal domain of APP (residues 646−695) with a C-terminal FLAG-myc-6xHis tandem tag. Anti-Nct monoclonal antibody A5226A, which recognizes an active form of Nct, was described previously.[22] The anti-PS1NT antibody was kindly provided by G. Thinakaran (The University of Chicago, Chicago, IL).[25] Other antibodies were purchased from Cell Signaling Technology [anti-cleaved Notch1 (V1744)], Covance [anti-Aph-1aL (O2C2)], Immuno-Biological Laboratories [anti-human APP (C)], or Sigma [anti-Nct (N1660) and anti-α-tubulin (DM1A)]. Membrane fractionation, immunoblot analysis, immunoprecipitation of 3-[(3-cholamidopropyl)-dimethylammonio]-2-hydroxy-1-propanesulfonate (CHAPSO)-solubilized lysates, immunocytochemistry, the in vitro γ-secretase assay, the cell-free γ-secretase assay, and quantitation of Aβ by two-site ELISAs were performed as previously described.[26−32] HEK293/SC100-gal4 cells and #5/DKO reporter cells for Aβ and luciferase assays, respectively, were plated on 96-well plates 24 h before the addition of the designated concentration of antibodies or DAPT (50 μM). The treated cell lysates were subjected to the luciferase measurement as previously described.[18] In the cell viability assay using A549, cells were plated in 96-well plates (5000 cells per well, 100 μL) 24 h before the addition of DAPT or mAb. After incubation for 96 h, 10 μL of Alamar Blue (Seretec, Oxford, U.K.) was added to each well and incubated for 3 h at 37 °C. Cell viability was calculated from the fluorescence value for Alamar Blue.[22]

Compounds, Substituted Cysteine Accessibility Method (SCAM), and Photoaffinity Labeling. *N*-biotinaminoethyl methanethiosulfonate (MTSEA-biotin) (Toronto Research Chemicals, Toronto, ON) was dissolved in DMSO at 200 mM and stored at −80 °C until use. 31C and 31C-Bpa were kindly provided by N. Umezawa and T. Higuchi (Nagoya City University, Aichi, Japan).[18] Peptide 11 (pep11) and pep11-Bt were purchased from Ito Life Science and BEX, respectively. *N*-[*N*-(3,5-Difluorophenacetyl)-L-alanyl]-(*S*)-phenylglycine *tert*-butyl ester (DAPT) and DAP-BpB were gifts from T. Fukuyama (The University of Tokyo).[33] In SCAM analysis, microsome pellets were resuspended in PBS and incubated with 9D11 or rat IgG (1 μg/mL) for 30 min at room temperature before being labeled with MTSEA-biotin. Further details about SCAM analysis have been previously described.[11] Photoaffinity labeling experiments were performed using microsome fractions from DKO cells expressing wild-type (wt) PS1 as previously described.[17,18,34]

RESULTS

9D11 Recognized the Juxtamembranous Residues of HL1 Proximal to TMD1 of PS1. We developed rat mAbs[16] targeting the juxtamembrane region at the extracellular side of TMD1 using GST fused to residues K101−M139 of PS1 corresponding to HL1. We isolated mAb clone 9D11 of the IgG2b isotype that specifically reacted with synthetic peptides that included K101 or S102; the latter results suggest that the epitope of 9D11 sits at the most N-terminal residues of PS1

dx.doi.org/10.1021/bi301252r | *Biochemistry* 2013, 52, 61−69

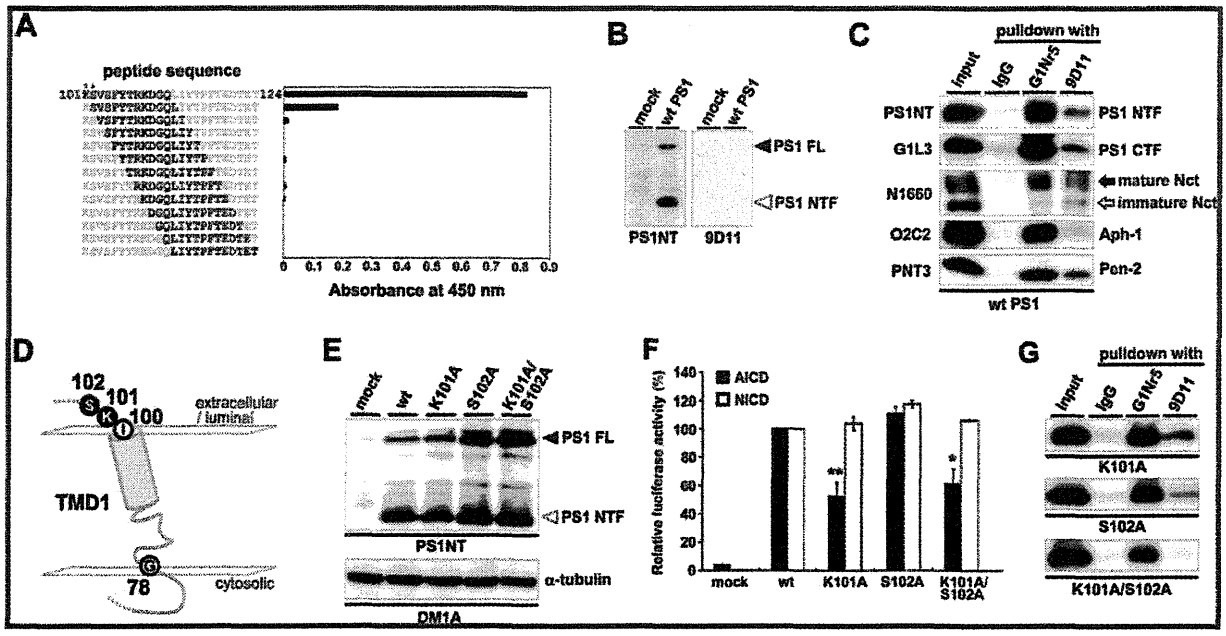

Figure 1. Reactivity of 9D11 against the γ-secretase complex. (A) The reactivity of 9D11 with the coated 12-mer synthetic sequential peptides encompassing residues K101–T124 of PS1 with an 11-amino acid overlap (black letters) was measured via sandwich ELISA analysis. The absorbance at 450 nm is represented as the length of the parallel line. The amino acids included specifically in the peptides with which 9D11 reacted are denoted with asterisks. (B) Immunoblot analysis of the lysates from DKO cells expressing mock or wt PS1 using PS1NT and 9D11: FL, full length; NTF, N-terminal fragment. (C) Immunoprecipitation analysis of the wt PS1-containing γ-secretase complex in CHAPSO lysate of DKO cells expressing wt PS1. Used antibodies are indicated above the lanes. Immunoblot analyses were performed with antibodies indicated at the left: CTF, C-terminal fragment. (D) Schematic illustration of TMD1 of PS1. TMD1 is comprised of residues G78–I100 (indicated in the white circles). K101 and S102 are shown in the black circles. (E) Immunoblot analysis of Ala mt PS1 expressed in DKO cells. (F) Luciferase reporter analysis using DKO cells expressing APP and Notch luciferase reporters transiently transfected with wt or Ala mt PS1. Firefly and renilla luciferase activities reflecting the amount of generated AICD (black bars) and NICD (white bars) were measured ($n = 3$; mean ± SEM; $*p < 0.05$; $**p < 0.01$). (G) Reactivity of 9D11 against Ala mt PS1 in immunoprecipitation using CHAPSO-solubilized DKO cells expressing PS1 mutants. Immunoblot analyses were performed with anti-PS1NT.

HL1 (Figure 1A). 9D11 did not react with holoprotein or fragment forms of PS1 upon immunoblot analysis of lysates from DKO cells stably expressing wild-type (wt) PS1, indicating that 9D11 is unable to react with the denatured PS1 polypeptide (Figure 1B). In contrast, 9D11 immunoprecipitated PS1 fragments from CHAPSO-solubilized DKO cells stably expressing wt PS1 lysates, in which the enzymatic activity as well as the integrity of the γ-secretase complex is retained. Furthermore, other components of the γ-secretase complex (i.e., Nct, Aph-1, and Pen-2) were successfully detected in the 9D11-precipitated fractions (Figure 1C). These data suggest that 9D11 recognizes PS1 within the γ-secretase complex.

9D11 recognizes the juxtamembranous residues of HL1 proximal to TMD1, which is comprised of residues G78–I100 of PS1 with the type II orientation (Figure 1D).[15] To test whether residues (K101 and S102) were critical for the immunoreactivity against 9D11, we performed co-immunoprecipitation experiments with lysates of DKO cells stably expressing mutant PS1 carrying one or two alanine substitutions (Ala mt PS1) at K101 and S102. These mutants were expressed and endoproteolyzed like wt PS1 (Figure 1E). In addition, Ala mt PS1 exhibited γ-secretase activity in luciferase reporter-expressing DKO cell lines[18] (Figure 1F). Notably, the production of the APP intracellular domain (AICD) in cells expressing PS1 carrying the K101A mutation or the K101A/S102A double mutation was specifically reduced, whereas that of the Notch intracellular domain (NICD) was not altered. 9D11 failed to react with the double-mutant Ala mt PS1 (K101A/S102A), while the single-mutant Ala mt PS1 (K101A and S102A) proteins were immunoprecipitated with 9D11 (Figure 1G). These results indicate that residues K101 and S102 of PS1 comprise the epitope of 9D11.

9D11 Inhibited the γ-Secretase Activity in Cultured Cells. γ-Secretase cleaves membrane-tethered substrates to secrete short peptides to the extracellular side (i.e., Aβ) and release intracellular domains to the cytosol [i.e., intracellular domain of APP and Notch (AICD and NICD, respectively)]. To examine whether 9D11 alters the γ-secretase activity, we first tested the AICD and NICD generation from DKO cells expressing direct γ-substrates. We found that the production of both proteolytic fragments was inhibited in a concentration-dependent manner (Figure 2A,B). Interestingly, the inhibitory effect of 9D11 was totally abolished in DKO cells expressing K101A/S102A mt PS1 (Figure 2C,D), indicating that K101 and S102 of PS1 are critical residues for recognition by 9D11 in living cells. Notably, the effect of 9D11 on Aβ secretion was significantly weaker than that on ICD generation (Figure 2E), supporting the previous notion that major subcellular compartments for Aβ and ICD generation are distinct.[35] These results prompted us to test whether the neutralizing activity of 9D11 is applicable for cancer therapeutics. We analyzed the cytotoxic effect of 9D11 against A549 cells derived from non-small cell lung cancer, which are known to be sensitive to GSIs.[22,36] DAPT, a representative small compound GSI, inhibited the

dx.doi.org/10.1021/bi301252r | Biochemistry 2013, 52, 61–69

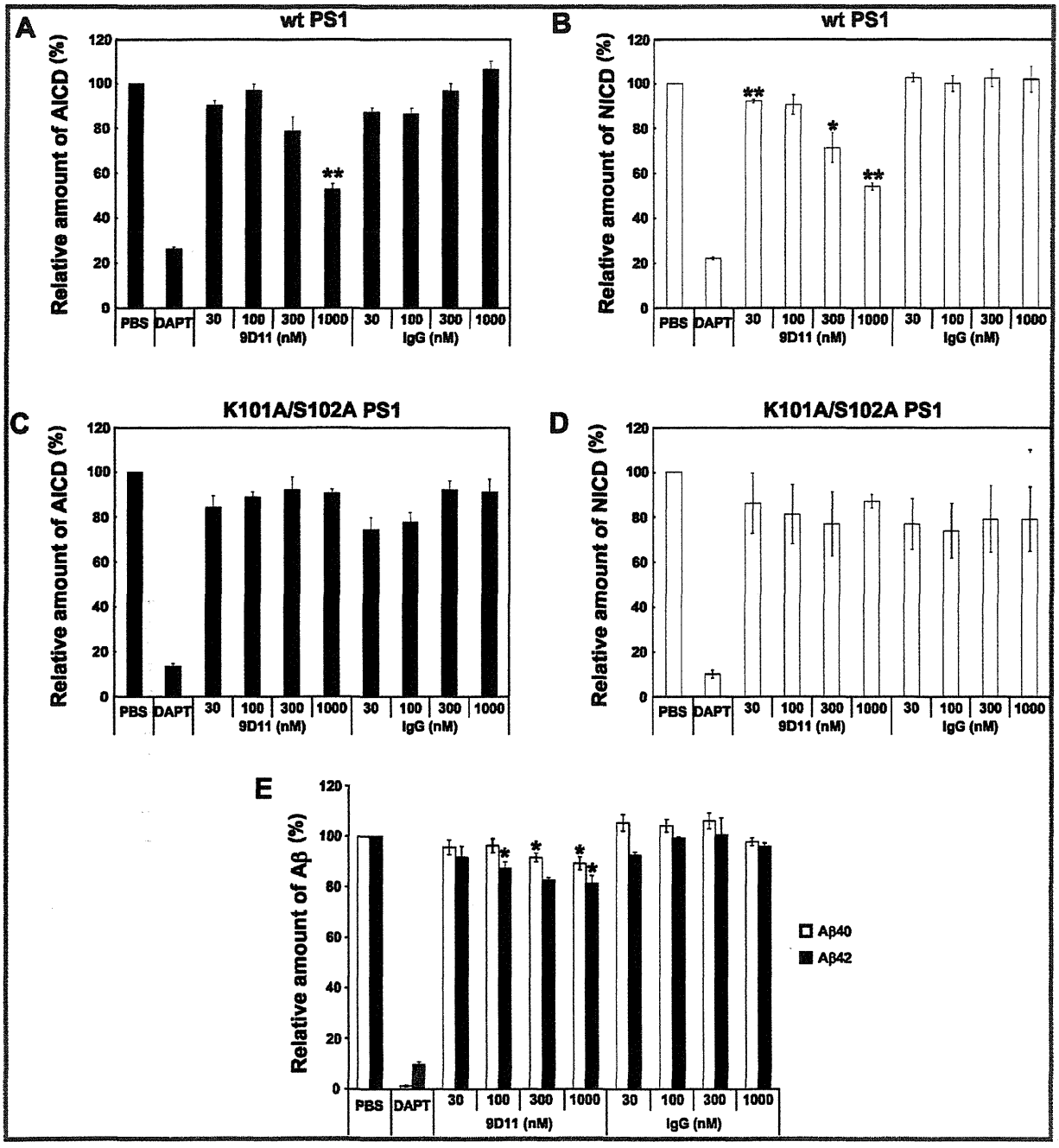

Figure 2. Effects of 9D11 on the γ-secretase activity of living cells. (A and B) Effects of 9D11 on the production ratio of AICD and NICD in a cell-based γ-secretase assay. DKO cells expressing APP and Notch luciferase reporters were transiently transfected with wt PS1. AICD (A) and NICD (B) levels are indicated by black and white bars, respectively (n = 3; mean ± SEM; $^*p < 0.05$; $^{**}p < 0.01$ against control rat IgG at each concentration). Values for DAPT (10 μM) or IgG are shown as controls. (C and D) Effects of 9D11 on K101A/S102A PS1-containing γ-secretase activity in a cell-based γ-secretase assay using reporter cells transfected with K101A/S102A PS1 (n = 3; mean ± SEM). Values for DAPT (10 μM) or IgG are shown as controls. (E) Effects of 9D11 on the production ratio of Aβ in a cell-based γ-secretase assay. Secreted Aβ in cultured media was analyzed by sandwich ELISAs (n = 3; mean ± SEM; $^*p < 0.05$ against control rat IgG at each concentration).

survival of A549 cells as previously reported.[22] Furthermore, 9D11 significantly reduced the viability of A549 cells, which was not affected by rat IgG (Figure 3). These data support our notion that 9D11 inhibits the γ-secretase on the surface of living cells and inhibits the intramembrane cleaving activity by targeting residues K101 and S102 of PS1.

Next we examined the molecular effect of 9D11. We did not observe any significant change in the localization of endogenous Nct in HeLa cells treated with 9D11, which was probed by monoclonal antibody A5226A that recognizes an active γ-secretase complex[22] (Figure 4A). Moreover, 9D11 treatment did not alter the levels of the N-terminal fragment

dx.doi.org/10.1021/bi301252r | Biochemistry 2013, 52, 61−69

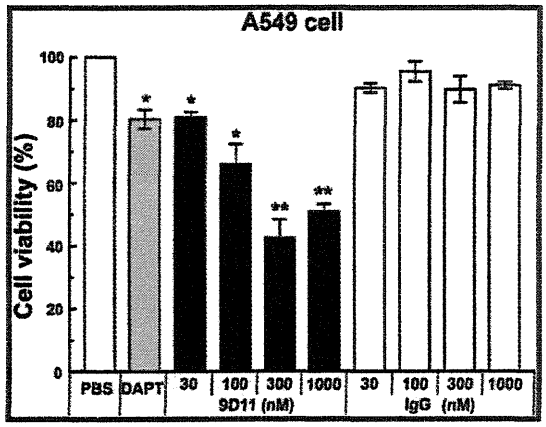

Figure 3. Effect of 9D11 on the viability of A549 cells. A549 cells were treated with 9D11, rat IgG, or DAPT (50 μM), and the cell viability was measured by the Alamar Blue assay (n = 3; mean ± SEM; *p < 0.05; **p < 0.01 against control rat IgG at each concentration or DMSO for DAPT).

that represents an active form of PS1 (Figure 4B),[6] suggesting that 9D11 did not affect the localization or the amount of the active γ-secretase by direct targeting of the enzyme. To gain further insight into the mechanism of the inhibitory effect of 9D11, we performed cross-competition experiments of the photoaffinity labeling of PS1 by small compound GSI-based probes.[18] We utilized three photoaffinity probes that target different molecular sites within PS1: 31C-Bpa for the catalytic site,[37] pep11-Bt for the initial substrate-binding site,[38] and DAP-BpB for the transit path that connects the substrate-binding and catalytic sites of the γ-secretase.[39] Preincubation of 9D11 showed no change in the binding of the photoprobe to PS1 (Figure 4C), suggesting that inhibition of the γ-secretase activity by 9D11 was achieved without affecting the structural integrity of the enzymatically functional sites within PS1. In addition, 9D11 failed to inhibit the intrinsic γ-secretase activity under a CHAPSO-solubilized condition (Figure 4D–F), while the level of AICD production was significantly decreased by 9D11 under detergent-free conditions (Figure 4G,H). These results raise the possibility that the membrane-embedded structure of PS1 is required for the inhibitory activity of 9D11.

To test whether the binding of 9D11 affects the structure of PS1, we applied SCAM analysis, in which the water accessibility of each amino acid residue was evaluated by the efficiency of labeling of MTSEA-biotin with each substituted cysteine residue.[11,12,15] Using this method, we have previously shown that small compound GSIs (i.e., L-685,458, pep15, and DAPT) caused the stabilization of the position of TMD1 that was evidenced by the coordinated reciprocal changes in the reactivity of G78C and I100C to MTSEA-biotin. Intriguingly, the labeling efficiency of G78C was increased, whereas that of I100C was decreased, by the preincubation with 9D11, in a manner similar to that observed with GSIs (Figure 5A).[15] These data indicate that the binding of mAb 9D11 to the juxtamembranous residues at the TMD1–HL1 border caused a structural change similar to that induced by known GSIs (Figure 5B). Moreover, 9D11 did not have any effects on the labeling efficiencies of E71C at the N-terminal extracellular domain of TMD1 and L383C in the catalytic pore. Notably, the hydrophilicity of L383C was decreased by L-685,458 and DAPT,[11] suggesting the local effect of 9D11 on the TMD1 positioning in the membrane. Taken together, our data suggest that 9D11 functions as an allosteric mAb that inhibits the γ-secretase activity in situ via stabilization of PS1 structure as an inhibitory conformation within the membrane.

DISCUSSION

To date, the correlation of structural dynamics with the enzymatic activity of PS/γ-secretase has never been achieved. In contrast, the structural dynamics of the rhomboid protease has been analyzed, and the motion of L1 loop and TMD5, the latter being closely located to the catalytic site, has been implicated in the gating of lateral substrate entry.[40,41] These reports suggest that the dynamic motion of the TMD and connecting loop would be critical for the proteolysis by intramembrane-cleaving proteases. Here we identified a mAb 9D11 targeting juxtamembrane residues at the TMD1–HL1 border of PS1 as an inhibitory antibody against γ-secretase. Using SCAM analysis, we have found that 9D11 caused the structural change of TMD1 in a manner similar to that of GSI treatment, while the binding sites of these compounds are distinct[15] (see Figure 4C). These data strongly support our notion that the TMD1–HL1 border is involved in the intramembrane-cleaving mechanism.

Biochemical studies revealed that all GSIs investigated so far target PS.[5] However, no inhibitory antibody against PS was reported, while some anti-Nct antibodies have been identified as neutralizing mAbs.[22,42,43] 9D11 is the first mAb targeting PS1 that regulates the γ-secretase activity. We found that K101 and S102 comprise the epitope of 9D11. These residues were conserved only in vertebrates, not in other species. Also, alanine substitutions of these residues did not deactivate the γ-secretase activity, suggesting that these residues are not essential for γ-secretase function. In contrast, our SCAM analysis revealed that 9D11 affected the water accessibility of the juxtamembrane residues of TMD1. Importantly, we have previously reported that the hydrophilicity of the TMD1 border was altered by GSIs.[15] Notably, the position of the TMD in the membrane is critical for the gating of several membrane-embedded channel/pore structures.[44–47] Moreover, recently, X-ray crystallographic analyses of the A_{2A} adenosine receptor as well as the β2 adrenergic receptor bound with antibody fragments were reported.[48,49] These antibody fragments stabilized the receptor structure in inactive and active states irrespective of ligand binding. Intriguingly, these antibodies targeted the TMD–HL border from the cytosolic side of the receptors, thereby allosterically affecting the structure of the ligand binding sites at the luminal side. Thus, it is plausible that the position of TMD1 in the membrane is affected by 9D11 in a manner similar to that of GSIs, leading to the loss of the γ-secretase activity by stabilization of the PS1 conformation as an inhibitory state (Figure 5B). However, we are unable to exclude the possibility that the steric hindrance effect of 9D11 is also involved in the inhibitory mechanism. Nevertheless, this report supports the view that the activity of transmembrane proteins would be regulated by allosteric modulation of the conformation of TMDs.

Here we show that 9D11 inhibits the γ-secretase activity in cultured cells, as well as the viability of cancer cells. These data suggest that the juxtamembrane region of TMD1 is a novel therapeutic target for the development of the treatments against some types of cancer, in which Notch signaling is required for proliferation. However, the use of 9D11 for therapeutics against Alzheimer's disease may not be directly feasible, as penetration

dx.doi.org/10.1021/bi301252r | Biochemistry 2013, 52, 61–69

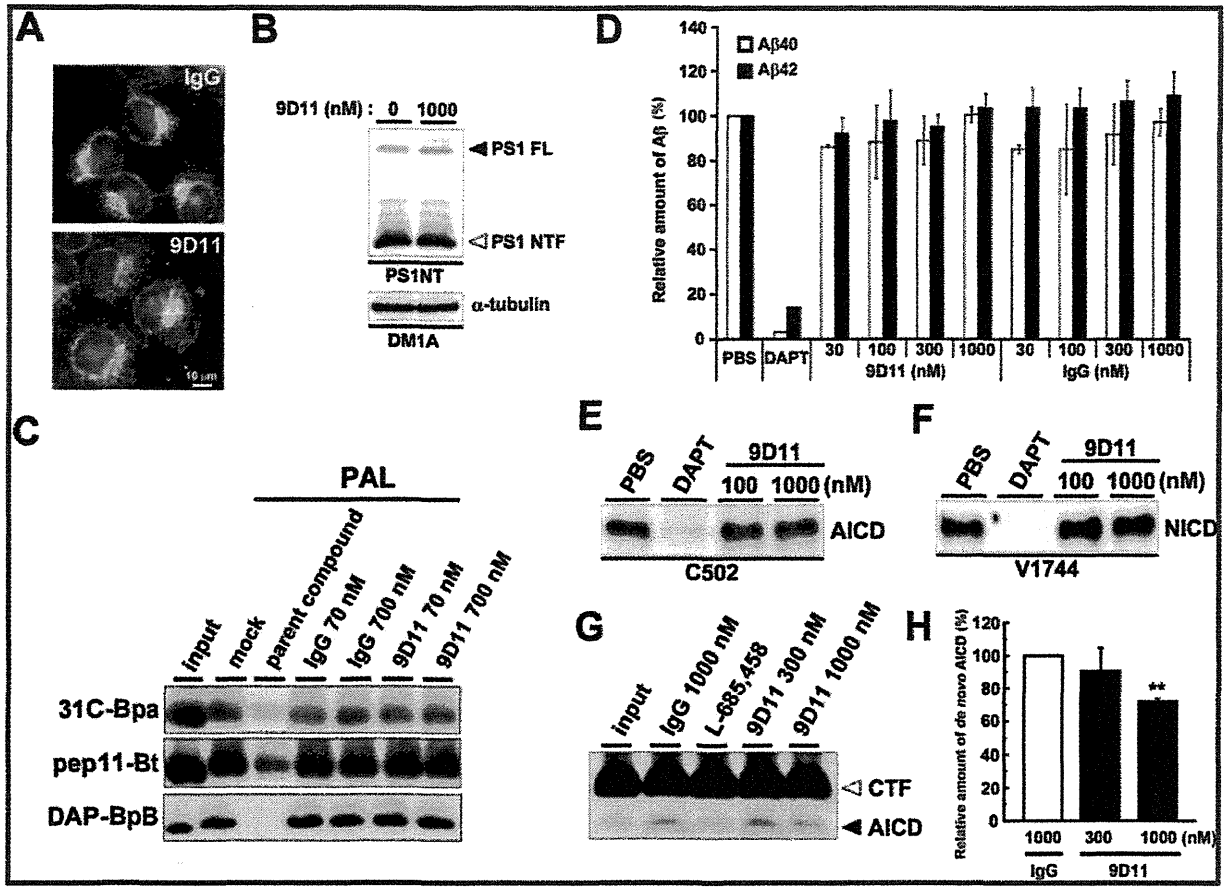

Figure 4. Mode of action of the inhibitory effect of 9D11. (A) Immunocytochemical analysis of HeLa cells treated with 9D11 or rat IgG (1 μM) for 24 h. Endogenous Nct was visualized by A5226A. (B) Effect of 9D11 on the level of expression of PS1 in DKO cells expressing wt PS1. (C) Competition assay against photoaffinity labeling (PAL) with 31C-Bpa, pep11-Bt, and DAP-BpB in the presence of rat IgG or 9D11. 31C, pep11, and DAPT were used as parent compounds for labeling with 31C-Bpa, pep11-Bt, and DAP-BpB, respectively. The biotinylated PS1 NTF was detected by immunoblotting analysis using anti-PS1NT. (D–F) Effect of 9D11 in the in vitro γ-secretase assay. Membranes of DKO cells expressing wt PS1 were solubilized with CHAPSO and co-incubated with recombinant substrate C100-FmH (D and E) or N102-FmH (F)[27] in the presence of 9D11. De novo Aβ generation was analyzed by a sandwich ELISA (n = 3; mean ± SEM) (D). AICD (E) and NICD (F) production were detected by using antibodies indicated below the panels. (G and H) Effect of 9D11 in the cell-free γ-secretase assay. Membranes from HeLa cells were incubated with rat IgG, L-685,458 (10 μM), or 9D11 under detergent-free conditions. De novo AICD generation and retained CTF were detected by anti-APP(C). The quantitation of de novo AICD levels is shown (H) (n = 3; mean ± SEM; $^{**}p < 0.01$ against control rat IgG).

of the blood–brain barrier by mAb is quite poor, and Notch signaling was also abolished by this mAb. Moreover, the inhibitory activity against Aβ generation was lower than that for AICD/NICD generation (Figure 2). This result would support the previous notion that major subcellular compartments for Aβ and ICD generation are distinct.[35] Importantly, AICD can be released from both C83 and C99 of APP, which are generated by α-secretase at the cell surface and β-secretase at the endosomal compartment, respectively. Thus, it would be plausible that 9D11 preferentially targets the γ-secretase complex at the cell surface, although we failed to probe 9D11-bound PS1 by conventional immunocytochemistry (data not shown). Alternatively, 9D11 is ineffective with or dissociates from PS1 at the endosomal compartment, where BACE1 generates C99. Nevertheless, modification of 9D11 as a probe for active PS1 would reveal a novel molecular aspect of γ-secretase-mediated cleavage. In addition, we found that PS1/K101A specifically inhibited APP cleavage, while NICD production was retained. We have reported a similar substrate-selective activity in cells expressing PS1/F86C, suggesting that TMD1 is a critical domain for substrate selectivity.[15] Thus, molecular engineering of 9D11 or selective targeting of TMD1 may lead to the generation of substrate-specific modulatory mAbs. Moreover, the effect of 9D11 on the generation of p3 and Nβ, which are derived from C83 and Notch proteins, respectively, by γ-secretase-mediated cleavage, would provide mechanistic insight into the substrate recognition by the γ-secretase. In conclusion, identification of 9D11 as an inhibitory mAb strengthened our hypothesis that TMD1 of PS1 plays an important role(s) in the catalytic activity in the substrate cleaving process. Further integrated analysis (i.e., X-ray crystallography and molecular dynamics simulation) will facilitate our understanding of the motion–activity relationships of PS1.

dx.doi.org/10.1021/bi301252r | *Biochemistry* 2013, 52, 61–69

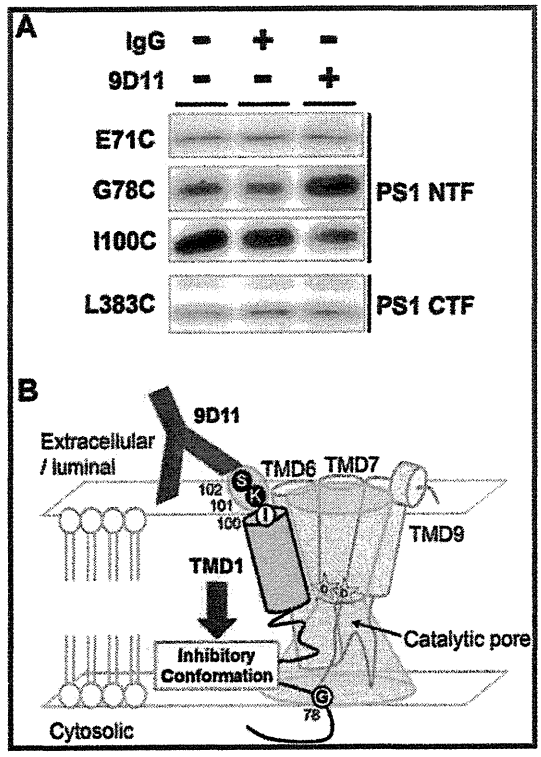

Figure 5. Effect of 9D11 on the vertical motion of TMD1 of PS1. (A) SCAM analysis of Cys-less PS1 carrying the E71C, G78C, I100C, or L383C mutation. Labeling by MTSEA-biotin was conducted after preincubation with 9D11 or rat IgG (70 nM). Labeled proteins were precipitated with streptavidin sepharose and detected by the anti-PS1NT antibody and G1L3 for PS1 NTF and CTF, respectively. Note that the hydrophilicities of G78 and I100 are simultaneously affected by 9D11 treatments. (B) Effect of 9D11 on PS1 structure. 9D11 targeting K101 and S102 (in green circles) decreased the γ-secretase activity by stabilizing TMD1 at the downward location in the membrane in a manner similar to that of GSIs. G78 and I100 used for SCAM analysis are indicated in white circles.

AUTHOR INFORMATION

Corresponding Author

*Department of Neuropathology and Neuroscience, Graduate School of Pharmaceutical Sciences, The University of Tokyo, Tokyo 113-0033, Japan. Phone: +81-3-5841-4868. E-mail: taisuke@mol.f.u-tokyo.ac.jp.

Author Contributions

S.T.-N. and T.T. designed the research. S.T.-N. and S.O. performed biochemical experiments. S.T.-N., T.T., and T.I. wrote the paper. All authors have given approval to the final version of the manuscript.

Funding

This work was supported in part by grants-in-aid for Young Scientists (S) from the Japan Society for the Promotion of Science (JSPS) (T.T.), by the Targeted Proteins Research Program of the Japan Science and Technology Corp. (JST) (T.T. and T.I.), and by Core Research for Evolutional Science and Technology of JST (T.T. and T.I.). S.T.-N. is a research fellow of JSPS.

Notes

The authors declare no competing financial interests.

ACKNOWLEDGMENTS

We thank Drs. B. De Strooper (Katholieke Universiteit Leuven, Leuven, Belgium), R. Kopan (Washington University at St. Louis, St. Louis, MO), U. Strobl (Helmholtz Zentrum Munchen, Munich, Germany), T. Kitamura, H. Arai, and T. Fukuyama (The University of Tokyo), N. Umezawa and T. Higuchi (Nagoya City University, Nagoya, Japan), K. I. Nakayama (Kyushu University, Fukuoka, Japan), and G. Thinakaran (The University of Chicago) for valuable reagents, Takeda Pharmaceutical Co. (Osaka, Japan) for the Aβ ELISA, J. Takagi (The University of Osaka, Osaka, Japan) for productive discussions, and our current and previous laboratory members for helpful discussions and technical assistance.

ABBREVIATIONS

Aβ, amyloid-β peptide; AICD, APP intracellular domain; Aph-1, anterior pharynx defective-1; DKO, *Psen1*$^{-/-}$/*Psen2*$^{-/-}$ double-knockout embryonic fibroblast; ELISA, enzyme-linked immunosorbent assay; GSI, γ-secretase inhibitor; HL, hydrophilic loop; Nct, nicastrin; NICD, Notch intracellular domain; mAb, monoclonal antibody; mt, mutant; MTSEA-biotin, *N*-biotinaminoethyl methanethiosulfonate; Pen-2, presenilin enhancer-2; PS, presenilin; S2P, site-2 protease; SCAM, substituted cysteine accessibility method; SEM, standard error of the mean; TMD, transmembrane domain; wt, wild-type.

REFERENCES

(1) Wolfe, M. S., and Kopan, R. (2004) Intramembrane proteolysis: Theme and variations. *Science 305*, 1119–1123.

(2) Holtzman, D. M., Morris, J. C., and Goate, A. M. (2011) Alzheimer's disease: The challenge of the second century. *Sci. Transl. Med. 3*, 77sr71.

(3) De Strooper, B., Iwatsubo, T., and Wolfe, M. S. (2012) Presenilins and γ-Secretase: Structure, Function, and Role in Alzheimer Disease. *Cold Spring Harbor Perspect. Med. 2*, a006304.

(4) Pannuti, A., Foreman, K., Rizzo, P., Osipo, C., Golde, T., Osborne, B., and Miele, L. (2010) Targeting Notch to target cancer stem cells. *Clin. Cancer Res. 16*, 3141–3152.

(5) Tomita, T. (2009) Secretase inhibitors and modulators for Alzheimer's disease treatment. *Expert Rev. Neurother. 9*, 661–679.

(6) Takasugi, N., Tomita, T., Hayashi, I., Tsuruoka, M., Niimura, M., Takahashi, Y., Thinakaran, G., and Iwatsubo, T. (2003) The role of presenilin cofactors in the γ-secretase complex. *Nature 422*, 438–441.

(7) Erez, E., Fass, D., and Bibi, E. (2009) How intramembrane proteases bury hydrolytic reactions in the membrane. *Nature 459*, 371–378.

(8) Kaback, H. R., Sahin-Toth, M., and Weinglass, A. B. (2001) The kamikaze approach to membrane transport. *Nat. Rev. Mol. Cell Biol. 2*, 610–620.

(9) Karlin, A., and Akabas, M. H. (1998) Substituted-cysteine accessibility method. *Methods Enzymol. 293*, 123–145.

(10) Seal, R. P., Leighton, B. H., and Amara, S. G. (1998) Transmembrane topology mapping using biotin-containing sulfhydryl reagents. *Methods Enzymol. 296*, 318–331.

(11) Sato, C., Morohashi, Y., Tomita, T., and Iwatsubo, T. (2006) Structure of the catalytic pore of γ-secretase probed by the accessibility of substituted cysteines. *J. Neurosci. 26*, 12081–12088.

(12) Sato, C., Takagi, S., Tomita, T., and Iwatsubo, T. (2008) The C-terminal PAL motif and transmembrane domain 9 of presenilin 1 are involved in the formation of the catalytic pore of the γ-secretase. *J. Neurosci. 28*, 6264–6271.

(13) Tolia, A., Chavez-Gutierrez, L., and De Strooper, B. (2006) Contribution of presenilin transmembrane domains 6 and 7 to a water-containing cavity in the γ-secretase complex. *J. Biol. Chem. 281*, 27633–27642.

(14) Tolia, A., Horre, K., and De Strooper, B. (2008) Transmembrane domain 9 of presenilin determines the dynamic conformation of the catalytic site of γ-secretase. *J. Biol. Chem. 283*, 19793–19803.
(15) Takagi, S., Tominaga, A., Sato, C., Tomita, T., and Iwatsubo, T. (2010) Participation of transmembrane domain 1 of presenilin 1 in the catalytic pore structure of the γ-secretase. *J. Neurosci. 30*, 15943–15950.
(16) Tanaka, M., Kishi, Y., Takanezawa, Y., Kakehi, Y., Aoki, J., and Arai, H. (2004) Prostatic acid phosphatase degrades lysophosphatidic acid in seminal plasma. *FEBS Lett. 571*, 197–204.
(17) Watanabe, N., Tomita, T., Sato, C., Kitamura, T., Morohashi, Y., and Iwatsubo, T. (2005) Pen-2 is incorporated into the γ-secretase complex through binding to transmembrane domain 4 of presenilin 1. *J. Biol. Chem. 280*, 41967–41975.
(18) Imamura, Y., Watanabe, N., Umezawa, N., Iwatsubo, T., Kato, N., Tomita, T., and Higuchi, T. (2009) Inhibition of γ-secretase activity by helical β-peptide foldamers. *J. Am. Chem. Soc. 131*, 7353–7359.
(19) Watanabe, N., Takagi, S., Tominaga, A., Tomita, T., and Iwatsubo, T. (2010) Functional analysis of the transmembrane domains of presenilin 1: Participation of transmembrane domains 2 and 6 in the formation of initial substrate-binding site of γ-secretase. *J. Biol. Chem. 285*, 19738–19746.
(20) Herreman, A., Serneels, L., Annaert, W., Collen, D., Schoonjans, L., and De Strooper, B. (2000) Total inactivation of γ-secretase activity in presenilin-deficient embryonic stem cells. *Nat. Cell Biol. 2*, 461–462.
(21) Kitamura, T., Koshino, Y., Shibata, F., Oki, T., Nakajima, H., Nosaka, T., and Kumagai, H. (2003) Retrovirus-mediated gene transfer and expression cloning: powerful tools in functional genomics. *Exp. Hematol. 31*, 1007–1014.
(22) Hayashi, I., Takatori, S., Urano, Y., Miyake, Y., Takagi, J., Sakata-Yanagimoto, M., Iwanari, H., Osawa, S., Morohashi, Y., Li, T., Wong, P. C., Chiba, S., Kodama, T., Hamakubo, T., Tomita, T., and Iwatsubo, T. (2012) Neutralization of the γ-secretase activity by monoclonal antibody against extracellular domain of nicastrin. *Oncogene 31*, 787–798.
(23) Tomita, T., Takikawa, R., Koyama, A., Morohashi, Y., Takasugi, N., Saido, T. C., Maruyama, K., and Iwatsubo, T. (1999) C terminus of presenilin is required for overproduction of amyloidogenic Aβ42 through stabilization and endoproteolysis of presenilin. *J. Neurosci. 19*, 10627–10634.
(24) Isoo, N., Sato, C., Miyashita, H., Shinohara, M., Takasugi, N., Morohashi, Y., Tsuji, S., Tomita, T., and Iwatsubo, T. (2007) Aβ42 overproduction associated with structural changes in the catalytic pore of γ-secretase: Common effects of Pen-2 N-terminal elongation and fenofibrate. *J. Biol. Chem. 282*, 12388–12396.
(25) Thinakaran, G., Regard, J. B., Bouton, C. M., Harris, C. L., Price, D. L., Borchelt, D. R., and Sisodia, S. S. (1998) Stable association of presenilin derivatives and absence of presenilin interactions with APP. *Neurobiol. Dis. 4*, 438–453.
(26) Hayashi, I., Urano, Y., Fukuda, R., Isoo, N., Kodama, T., Hamakubo, T., Tomita, T., and Iwatsubo, T. (2004) Selective reconstitution and recovery of functional γ-secretase complex on budded baculovirus particles. *J. Biol. Chem. 279*, 38040–38046.
(27) Morohashi, Y., Hatano, N., Ohya, S., Takikawa, R., Watabiki, T., Takasugi, N., Imaizumi, Y., Tomita, T., and Iwatsubo, T. (2002) Molecular cloning and characterization of CALP/KChIP4, a novel EF-hand protein interacting with presenilin 2 and voltage-gated potassium channel subunit Kv4. *J. Biol. Chem. 277*, 14965–14975.
(28) Takahashi, Y., Hayashi, I., Tominari, Y., Rikimaru, K., Morohashi, Y., Kan, T., Natsugari, H., Fukuyama, T., Tomita, T., and Iwatsubo, T. (2003) Sulindac sulfide is a noncompetitive γ-secretase inhibitor that preferentially reduces Aβ42 generation. *J. Biol. Chem. 278*, 18664–18670.
(29) Tomita, T., Maruyama, K., Saido, T. C., Kume, H., Shinozaki, K., Tokuhiro, S., Capell, A., Walter, J., Grunberg, J., Haass, C., Iwatsubo, T., and Obata, K. (1997) The presenilin 2 mutation (N141I) linked to familial Alzheimer disease (Volga German families) increases the secretion of amyloid β protein ending at the 42nd (or 43rd) residue. *Proc. Natl. Acad. Sci. U.S.A. 94*, 2025–2030.
(30) Tomita, T., Watabiki, T., Takikawa, R., Morohashi, Y., Takasugi, N., Kopan, R., De Strooper, B., and Iwatsubo, T. (2001) The first proline of PALP motif at the C terminus of presenilins is obligatory for stabilization, complex formation, and γ-secretase activities of presenilins. *J. Biol. Chem. 276*, 33273–33281.
(31) Tomita, T., Tanaka, S., Morohashi, Y., and Iwatsubo, T. (2006) Presenilin-dependent intramembrane cleavage of ephrin-B1. *Mol. Neurodegener. 1*, 2.
(32) Suzuki, K., Hayashi, Y., Nakahara, S., Kumazaki, H., Prox, J., Horiuchi, K., Zeng, M., Tanimura, S., Nishiyama, Y., Osawa, S., Sehara-Fujisawa, A., Saftig, P., Yokoshima, S., Fukuyama, T., Matsuki, N., Koyama, R., Tomita, T., and Iwatsubo, T. (2012) Activity-dependent proteolytic cleavage of neuroligin-1. *Neuron 76*, 410–422.
(33) Kan, T., Tominari, Y., Morohashi, Y., Natsugari, H., Tomita, T., Iwatsubo, T., and Fukuyama, T. (2003) Solid-phase synthesis of photoaffinity probes: Highly efficient incorporation of biotin-tag and cross-linking groups. *Chem. Commun.*, 2244–2245.
(34) Ohki, Y., Higo, T., Uemura, K., Shimada, N., Osawa, S., Berezovska, O., Yokoshima, S., Fukuyama, T., Tomita, T., and Iwatsubo, T. (2011) Phenylpiperidine-type γ-secretase modulators target the transmembrane domain 1 of presenilin 1. *EMBO J. 30*, 4815–4824.
(35) Tarassishin, L., Yin, Y. I., Bassit, B., and Li, Y. M. (2004) Processing of Notch and amyloid precursor protein by γ-secretase is spatially distinct. *Proc. Natl. Acad. Sci. U.S.A. 101*, 17050–17055.
(36) Luistro, L., He, W., Smith, M., Packman, K., Vilenchik, M., Carvajal, D., Roberts, J., Cai, J., Berkofsky-Fessler, W., Hilton, H., Linn, M., Flohr, A., Jakob-Rotne, R., Jacobsen, H., Glenn, K., Heimbrook, D., and Boylan, J. F. (2009) Preclinical profile of a potent γ-secretase inhibitor targeting notch signaling with in vivo efficacy and pharmacodynamic properties. *Cancer Res. 69*, 7672–7680.
(37) Micchelli, C. A., Esler, W. P., Kimberly, W. T., Jack, C., Berezovska, O., Kornilova, A., Hyman, B. T., Perrimon, N., and Wolfe, M. S. (2003) γ-Secretase/presenilin inhibitors for Alzheimer's disease phenocopy Notch mutations in Drosophila. *FASEB J. 17*, 79–81.
(38) Kornilova, A. Y., Bihel, F., Das, C., and Wolfe, M. S. (2005) The initial substrate-binding site of γ-secretase is located on presenilin near the active site. *Proc. Natl. Acad. Sci. U.S.A. 102*, 3230–3235.
(39) Morohashi, Y., Kan, T., Tominari, Y., Fuwa, H., Okamura, Y., Watanabe, N., Sato, C., Natsugari, H., Fukuyama, T., Iwatsubo, T., and Tomita, T. (2006) C-terminal fragment of presenilin is the molecular target of a dipeptidic γ-secretase-specific inhibitor DAPT (N-[N-(3,5-difluorophenacetyl)-L-alanyl]-S-phenylglycine t-butyl ester). *J. Biol. Chem. 281*, 14670–14676.
(40) Baker, R. P., Young, K., Feng, L., Shi, Y., and Urban, S. (2007) Enzymatic analysis of a rhomboid intramembrane protease implicates transmembrane helix 5 as the lateral substrate gate. *Proc. Natl. Acad. Sci. U.S.A. 104*, 8257–8262.
(41) Bondar, A. N., del Val, C., and White, S. H. (2009) Rhomboid protease dynamics and lipid interactions. *Structure 17*, 395–405.
(42) Zhang, X., Hoey, R. J., Lin, G., Koide, A., Leung, B., Ahn, K., Dolios, G., Paduch, M., Ikeuchi, T., Wang, R., Li, Y. M., Koide, S., and Sisodia, S. S. (2012) Identification of a tetratricopeptide repeat-like domain in the nicastrin subunit of γ-secretase using synthetic antibodies. *Proc. Natl. Acad. Sci. U.S.A. 109*, 8534–8539.
(43) Filipovic, A., Gronau, J. H., Green, A. R., Wang, J., Vallath, S., Shao, D., Rasul, S., Ellis, I. O., Yague, E., Sturge, J., and Coombes, R. C. (2011) Biological and clinical implications of nicastrin expression in invasive breast cancer. *Breast Cancer Res. Treat. 125*, 43–53.
(44) Gandhi, C. S., Clark, E., Loots, E., Pralle, A., and Isacoff, E. Y. (2003) The orientation and molecular movement of a K^+ channel voltage-sensing domain. *Neuron 40*, 515–525.
(45) Hazelbauer, G. L., and Lai, W. C. (2010) Bacterial chemoreceptors: Providing enhanced features to two-component signaling. *Curr. Opin. Microbiol. 13*, 124–132.

(46) Moller, J. V., Nissen, P., Sorensen, T. L., and le Maire, M. (2005) Transport mechanism of the sarcoplasmic reticulum Ca^{2+}-ATPase pump. *Curr. Opin. Struct. Biol. 15*, 387–393.
(47) Spijker, P., Vaidehi, N., Freddolino, P. L., Hilbers, P. A., and Goddard, W. A., III (2006) Dynamic behavior of fully solvated β2-adrenergic receptor, embedded in the membrane with bound agonist or antagonist. *Proc. Natl. Acad. Sci. U.S.A. 103*, 4882–4887.
(48) Hino, T., Arakawa, T., Iwanari, H., Yurugi-Kobayashi, T., Ikeda-Suno, C., Nakada-Nakura, Y., Kusano-Arai, O., Weyand, S., Shimamura, T., Nomura, N., Cameron, A. D., Kobayashi, T., Hamakubo, T., Iwata, S., and Murata, T. (2012) G-protein-coupled receptor inactivation by an allosteric inverse-agonist antibody. *Nature 482*, 237–240.
(49) Rasmussen, S. G., Choi, H. J., Fung, J. J., Pardon, E., Casarosa, P., Chae, P. S., Devree, B. T., Rosenbaum, D. M., Thian, F. S., Kobilka, T. S., Schnapp, A., Konetzki, I., Sunahara, R. K., Gellman, S. H., Pautsch, A., Steyaert, J., Weis, W. I., and Kobilka, B. K. (2011) Structure of a nanobody-stabilized active state of the β(2) adrenoceptor. *Nature 469*, 175–180.

Journal of Medicinal Chemistry

Article

pubs.acs.org/jmc

Effect of Helical Conformation and Side Chain Structure on γ-Secretase Inhibition by β-Peptide Foldamers: Insight into Substrate Recognition

Yuki Imamura,[†] Naoki Umezawa,*[,†] Satoko Osawa,[‡] Naoaki Shimada,[§] Takuya Higo,[§] Satoshi Yokoshima,[§] Tohru Fukuyama,[§] Takeshi Iwatsubo,[‡,∥,⊥] Nobuki Kato,[†] Taisuke Tomita,*[,‡,∥] and Tsunehiko Higuchi*[,†]

[†]Department of Bioorganic-Inorganic Chemistry, Graduate School of Pharmaceutical Sciences, Nagoya City University, 3-1 Tanabe-dori, Mizuho-ku, Nagoya, Aichi, Japan

[‡]Department of Neuropathology and Neuroscience, Graduate School of Pharmaceutical Sciences, The University of Tokyo, 7-3-1 Hongo, Bunkyo-ku, Tokyo, Japan

[§]Department of Synthetic Natural Products Chemistry, Graduate School of Pharmaceutical Sciences, The University of Tokyo, 7-3-1 Hongo, Bunkyo-ku, Tokyo, Japan

[∥]Core Research for Evolutional Science and Technology (CREST), Japan Science and Technology Agency, Tokyo, Japan

[⊥]Department of Neuropathology, Graduate School of Medicine, The University of Tokyo, 7-3-1 Hongo, Bunkyo-ku, Tokyo, Japan

Supporting Information

ABSTRACT: Substrate-selective inhibition or modulation of the activity of γ-secretase, which is responsible for the generation of amyloid-β peptides, might be an effective strategy for prevention and treatment of Alzheimer's disease. We have shown that helical β-peptide foldamers are potent and specific inhibitors of γ-secretase. Here we report identification of target site of the foldamers by using a photoaffinity probe. The photoprobe directly and specifically labeled the N-terminal fragment of presenilin 1, in which the initial substrate docking site is predicted to be located. We also optimized the foldamer structure by preparing a variety of derivatives and obtained two highly potent foldamers by incorporation of a hydrophilic and neutral functional group into the parent structure. The class of side chain functional group and the position of incorporation were both important for γ-secretase-inhibitory activity. The substrate selectivity of the inhibitory activity was also quite sensitive to the class of side chain group incorporated.

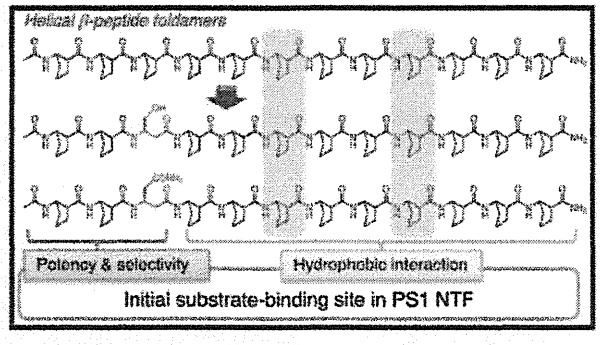

INTRODUCTION

Several lines of evidence suggest that aggregation and deposition of amyloid-β peptides (Aβ) underlie the pathogenesis of Alzheimer's disease (AD).[1] Aβ is a proteolytic fragment of amyloid precursor protein (APP) formed via sequential cleavages by two proteases, β- and γ-secretases. γ-Secretase determines the C-terminal length of Aβ, which in turn impacts on the aggregation properties of Aβ; the C-terminally longer Aβ42 is the initially deposited and most aggregation-prone species and is linked to the pathogenesis of AD.[2] Thus, γ-secretase has been a prime target for drug discovery, and many γ-secretase inhibitors (GSIs) have been developed.[3−7]

γ-Secretase is a complex of four integral membrane proteins, namely, presenilin (PS), nicastrin, Aph-1, and Pen-2.[8] PS serves as the catalytic subunit of γ-secretase, with a pair of catalytic aspartate residues being located on the N- and C-terminal endoproteolytic fragments of PS (NTF and CTF, respectively). A series of chemical−biological experiments indicated that reported GSIs can be classified into three categories based on the main enzymatically functional sites,[5] namely, the catalytic site (transition-state analogue),[9,10] the initial substrate docking site (helical peptide),[11,12] and the transition path or allosteric site.[13,14]

Conventional GSIs, however, have little therapeutic potential. γ-Secretase cleaves a wide variety of other substrates in addition to APP, including APP-like proteins 1 and 2, N- and E-cadherins, ErbB4, and Notch receptors.[15,16] Proteolysis of the Notch transmembrane domain by γ-secretase is an essential part of its signaling pathway, and blocking of this process by GSIs causes severe adverse effects, including gastrointestinal

Received: June 30, 2012
Published: January 23, 2013

toxicity and immunosuppression.[17,18] Thus, recent efforts in drug discovery have focused on identification of γ-secretase modulator and Notch-sparing GSIs, which would influence Aβ formation without affecting Notch processing.[3−7] γ-Secretase modulators do not change total Aβ production but rather shift the spectrum of generated Aβ species toward shorter forms, which are more soluble and less pathogenic. On the other hand, Notch-sparing GSIs would inhibit cleavage of APP in a substrate-selective manner, blocking the production of all Aβs while allowing Notch proteolysis to occur.

Recently, we have identified several foldamers as GSIs.[12] Foldamers are sequence-specific oligomers of non-natural building blocks that adopt well-defined secondary and tertiary structures.[19−21] Helical β-peptide foldamers can mimic the structure of a transmembrane domain of C99, which is a direct γ-secretase substrate, and as a result, they potently inhibit γ-secretase activity.[12] Foldamer 1 is the most potent GSI among the foldamers we have synthesized (Figure 1b). Despite its simple structure, foldamer 1 did not inhibit membrane-bound metalloproteases ADAM9, -10, and -17 or signal peptide peptidase (SPP). Foldamers showed moderate substrate selectivity in a fashion similar to that of Notch-sparing GSIs. We considered that foldamer 1 is a potential lead compound for the development of APP-cleaving γ-secretase activity-specific inhibitors.

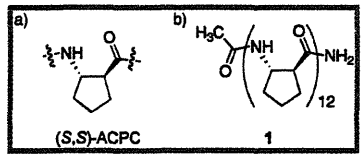

Figure 1. Structures of (a) (*S,S*)-ACPC and (b) foldamer 1.

As substrate-based inhibitors that target the initial substrate docking site, helical peptides containing multiple helix-inducing Aib (2-aminoisobutyric acid) residues have been reported.[22,23] We found that foldamers compete with Aib-containing peptide for binding to PS1 NTF, where the initial substrate docking site is located, suggesting that the foldamers may also target the initial binding site or allosterically affect the structure of PS1. Both Aib-containing L- and D-peptides potently inhibit γ-secretase activity, but in either case structural modifications that disrupt the helical conformation result in a dramatic reduction of inhibitory potency. A similar tendency was observed in the case of foldamers.[12] However, no systematic investigation on the effect of side chain functional groups has been reported. The helical peptides contained only a few different amino acids, such as valine, isoleucine, and threonine.[22,23] In general, short linear peptides tend not to form a stable helix because of their high intrinsic flexibility. Although the Aib residue is known to stabilize helical structure, formation of a highly stable helix is still difficult.[24,25] Thus, it would be problematic to incorporate side chain functional groups at specific positions of helical peptides. However, since even short foldamers have strong tendency to form a stable helix, helical foldamers should be an appropriate platform to examine the effect of side chain functional groups.

Here, we examined in detail the properties of foldamers as GSIs by synthesizing a series of compounds related to 1 in order to identify the optimum shape of the helix, the optimum length of the foldamer, and the enzyme target site of 1. We also report the design, synthesis, and γ-secretase-inhibitory activity of foldamer 1 derivatives with various side chain functional groups. Our findings provide information on substrate recognition by γ-secretase and are expected to be useful for the design of substrate-selective GSIs.

RESULTS AND DISCUSSION

Shape of Helix. β-Peptides, which are oligomers of β-amino acids, represent an attractive unnatural scaffold because they adopt predictable helical conformations and resist proteolysis.[26] Our γ-secretase-inhibitory β-peptide foldamers were composed of (*S,S*)-2-aminocyclopentanecarboxylic acid (ACPC, Figure 1a) and form a stable 12-helix. The β-peptide 12-helix is defined by C=O(*i*)→H−N(*i*+3) hydrogen bonds that involve 12 atoms, and its formation is promoted by the use of β-residues with a five-membered ring constraint. Among the foldamers we synthesized, the (*S,S*)-ACPC dodecamer 1 showed the most potent inhibitory activity. The β-peptide 12-helix is a mimic of the α-helices seen in conventional peptides and proteins.[27,28] The internal hydrogen bond orientation and macrodipole are analogous to those of α-peptide helices (α-helix and 3_{10}-helix) but different from those of other β-peptide helices.[21] The β-peptide 12-helix repeats approximately every 2.5 residues.[21] The rise-per-turn of β-peptide 12-helix is 5.4 Å, which is about the same as the pitch of the α-helix and slightly smaller than that of the 3_{10}-helix (5.8 Å).[27−29] Thus, the β-peptide 12-helix seems to be the most appropriate candidate for an α-helix mimic, but nevertheless, other types of helical motif might also be potential GSIs. To examine this idea, we designed and synthesized a series of oligoproline peptides that are known to form a well-defined left-handed polyproline II (PPII) helix in polar solvents.[27] Polyproline display helical conformations in the absence of hydrogen bonding; PPII contains three residues per turn, aligning every third ring on the same face of the helix with a pitch of approximately 10 Å per turn.[27]

The synthesized oligoprolines are shown in Figure 2a. Oligomers of L- and D-proline were both synthesized. Circular dichroism (CD) spectra were measured in methanol (Figure 2b). The spectra of L-peptides 2−4 were all similar, showing minima at 205 nm and maxima at 228 nm, which are typical of

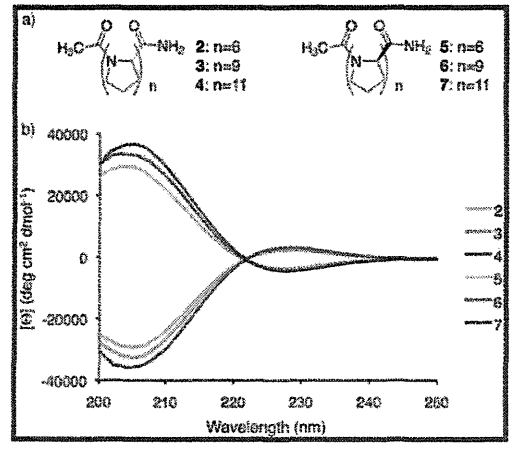

Figure 2. (a) Structures of oligoproline peptides. Peptides 2−4 are composed of L-proline, and 5−7 are composed of D-proline. (b) CD spectra of oligoproline peptides in methanol. The molar ellipticity [Θ] values have been normalized for peptide concentration and the number of backbone amide groups.

dx.doi.org/10.1021/jm301306c | J. Med. Chem. 2013, 56, 1443−1454

the left-handed PPII helix.[30] The increase in intensity at 228 nm with addition of further proline residues indicates that the population of the PPII helical state increases as the peptide length increases. D-Peptides **5**–**7** had mirror-image CD spectra compared with their enantiomers **2**–**4** within experimental error, corresponding to a right-handed PPII helix.

The inhibitory potency of these oligoproline peptides was analyzed using an in vitro γ-secretase assay (Table 1).[31] None of the oligoprolines showed inhibitory activity, suggesting that 12-helical structure is important for γ-secretase inhibition.

Table 1. Inhibitory Potency of Oligoproline Peptides toward γ-Secretase in in Vitro Assay (n = 3)

	IC_{50} (nM)	
compd	$A\beta_{40}$	$A\beta_{42}$
2	>3.00 × 10^4	>3.00 × 10^4
3	>3.00 × 10^4	>3.00 × 10^4
4	>3.00 × 10^4	>3.00 × 10^4
5	>3.00 × 10^4	>3.00 × 10^4
6	>3.00 × 10^4	>3.00 × 10^4
7	>3.00 × 10^4	>3.00 × 10^4

Length of Foldamer. Next, we examined the most appropriate length of 12-helical foldamer. We have reported that foldamer **1** showed stronger activity than ACPC 9mer, but we did not evaluate ACPC 10mer and 11mer. Thus, foldamers **8** and **9** were synthesized and their inhibitory activity was examined (Figure 3a). Fmoc-(*S*,*S*)-ACPC-OH was efficiently

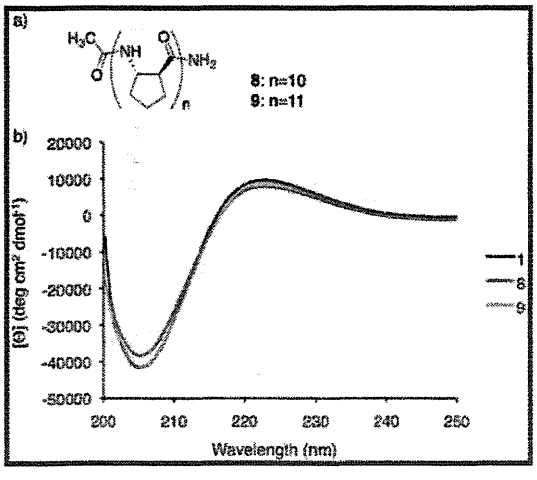

Figure 3. (a) Structure of foldamers **8** (10mer) and **9** (11mer). (b) CD spectra of foldamers **8** and **9** in methanol. The molar ellipticity [Θ] values have been normalized for peptide concentration and the number of backbone amide groups.

prepared from ethyl 2-oxocyclopentanecarboxylate according to the literature.[32] The foldamers were prepared by solid-phase methods analogous to the standard Fmoc solid-phase peptide synthesis and purified by preparative reverse-phase HPLC (for details, see Supporting Information). The folding propensities of these foldamers in methanol were examined by CD spectroscopy (Figure 3b). All foldamers, including foldamer **1**, displayed a maximum at 222 nm and a minimum at 204–205 nm, which are characteristic of right-handed 12-helical β-peptides.[33−35] The increase in intensity at 222 nm with addition of further ACPC residues indicates that the population of 12-helical state increases; i.e., the stability of this helical state increases as the length of the foldamer is increased. Foldamers **1** (12mer) and **9** (11mer) showed similar spectra, suggesting that the 11mer is sufficiently long to achieve a high population of the 12-helical state. In order to clarify the inhibitory potency precisely, the IC_{50} values were measured using an in vitro assay.[31] As shown in Table 2, foldamer **1** was the most potent

Table 2. Inhibitory Potency of Foldamers toward γ-Secretase in in Vitro Assay (n = 3)

		IC_{50} (nM)	
compd	no. of β-amino acids	Aβ40	Aβ42
1	12	8.81 ± 1.05	9.93 ± 2.14
8	10	2280 ± 118	5210 ± 259
9	11	244 ± 20.0	225 ± 8.62

inhibitor, although foldamers **1** and **9** showed comparably high population of 12-helical state. We concluded that foldamer **1** is an appropriate lead structure for further modification.

Direct Identification of the Target Site. It is widely accepted that (1) PS fragments represent the proteolytically active molecule, (2) PS fragments form an initial substrate docking site that is distinct from the catalytic site of γ-secretase, and (3) substrates are transferred from the docking site to the catalytic site through a transition path.[14] Pep.11-Bt, a photoactivatable helical peptide containing Aib, is known to label PS1 NTF under photoirradiation (see Supporting Information for chemical structure).[11] The labeling of PS1 NTF by pep.11-Bt was completely abolished by preincubation with foldamer **1**, suggesting that **1** shares the same binding site with pep.11, namely, the initial substrate docking site.[12] However, we could not exclude the possibility that **1** allosterically altered the conformation of the pep.11-Bt binding site. Therefore, we set out to directly identify the target site by employing a photoactivatable analogue of **1**.

To create the photoprobe, we modified foldamer **1** by incorporating 4-benzoyl-L-phenylalanine (Bpa) at the N-terminus. We also installed biotin via a linker module at the N terminus to generate **10** (Figure 4a). The side chain of the Bpa residue is benzophenone, a commonly used photoreactive moiety that is covalently inserted into the closest C–H bond (within 3 Å) upon irradiation at 350 nm.[36] Biotin allows isolation of the labeled species with avidin-based beads. Synthesis of **10** was performed by a solid-phase method, and the product was purified by reverse-phase HPLC. The CD spectrum of **10** confirmed that it retained the right-handed 12-helical structure, although the population of 12-helix was decreased compared with **1** (see Supporting Information). Also, foldamer **10** retained a significant γ-secretase-inhibitory activity, although the activity was weaker than that of **1** (see Supporting Information).

CHAPSO-solubilized cell lysates were incubated with foldamer **10** in the presence or absence of the parent foldamer **1** and irradiated at 350 nm. The photolabeled proteins were pulled down with streptavidin beads and subjected to immunoblotting. As shown in Figure 4b, foldamer **10** specifically labeled PS1 NTF in the same manner as did pep.11-Bt, and the labeling was subject to competition by an excess of the parent foldamer **1**. In addition, we never observed the labeling of PS1 CTF, which is a direct molecular target of dipeptidic GSI DAPT-based photoprobe DAP-BpB (Figure

dx.doi.org/10.1021/jm301306c | J. Med. Chem. 2013, 56, 1443–1454

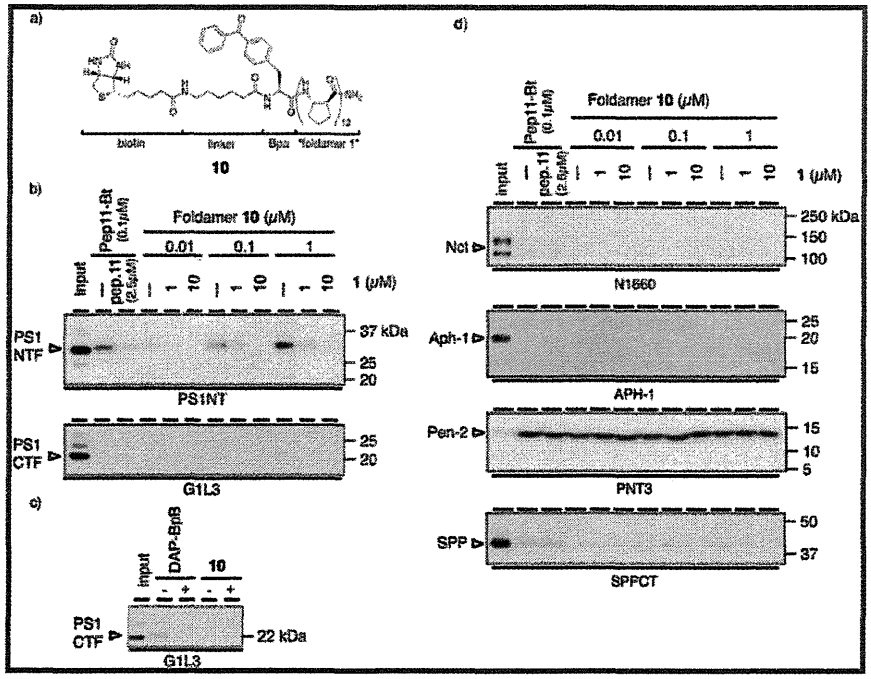

Figure 4. (a) Structure of **10**, which incorporates biotin and benzophenone. (b–d) Photoaffinity labeling experiment with **10** and competition assay in the presence of **1**. Labeling by pep.11-Bt (b, d) or DAP-BpB (c) with/without parent compound (pep.11 or DAPT, respectively) is shown as control experiments. Antibodies used are shown under the panels. Nonspecific interaction of Pen-2 with both photoprobes was observed.

4c).[14] In contrast, we did not observe specific labeling of other γ-secretase components (i.e., PS1 CTF, nicastrin, Aph-1, and Pen-2; Figure 4b,d). We also investigated the labeling of signal peptide peptidase (SPP), an intramembrane cleaving protease that shares catalytic YD/GxGD motifs with PS.[37] We and others have reported that transition state analogue-type GSIs, as well as potent dipeptidic GSIs such as DBZ but not DAPT, cross-inhibit SPP.[13,38,39] It is noteworthy that leucine-rich Aib-containing helical peptides, although their sequence is different from that of pep.11, cross-inhibited γ-secretase and SPP activities.[40,41] In fact, pep.11-Bt also bound to SPP in our assay. However, no specific photolabeling of SPP by photoprobe **10** was observed (Figure 4d), in good accordance with our previous finding that foldamer **1** did not inhibit SPP.[12] Taken together, these results strongly indicate that foldamer **1** directly targets the initial substrate docking site in PS.

Modification of Foldamer 1. Foldamer **1** seemed the most appropriate candidate for structural modification. Although the cyclopentane unit in ACPC residue is hydrophobic, the chemical structure of **1** is extremely simple and contains no significant functional group. We envisioned that replacement of the ACPC residue with a β^3-amino acid with a side chain functional group might improve the inhibitory potency and/or substrate selectivity. The strong folding propensity of β-peptide foldamer was expected to ensure that the overall conformation would be maintained after the incorporation of functional group(s), which is not necessarily the case with α-peptides; short α-peptides normally do not form stable helices. Precise design and rapid solid-phase synthesis are feasible with the β-peptide foldamer scaffold. Since β-peptide foldamers are not susceptible to proteolytic degradation,[26,42] foldamer **1** should be a good lead compound not only for development of chemical tools for biomedical research but also for candidate pharmaceuticals active in vivo.

We designed foldamers **11–25** by replacing an ACPC residue with a linear β^3-amino acid bearing a proteinogenic side chain functional group (Figure 5a). ACPC oligomers are known to maintain their 12-helical conformation even when some of the rigid ACPC residues are replaced with linear, flexible β^3-amino acids.[29,43] We chose five different β^3-amino acids with representative side chain functional groups, namely, β^3-hSer, β^3-hAsn, β^3-hGlu, β^3-hLys, and β^3-hLeu. These β^3-amino acids contain neutral and hydrophilic (β^3-hSer, β^3-hAsn), negatively charged (β^3-hGlu), positively charged (β^3-hLys), and hydrophobic (β^3-hLeu) functional groups. To clarify the appropriate position of replacement, we synthesized foldamer **1** in which the residue at the third (X_3), sixth (X_6), or ninth (X_9) position was replaced with one of the above β^3-amino acids.

Fmoc-β^3-amino acids, which are suitably protected for solid-phase synthesis, were prepared enantiospecifically from the corresponding Fmoc-α-amino acids via methodology developed by Seebach et al.,[44] as modified by Müller et al.[45] The obtained compounds showed spectroscopic data identical to those reported in the literature.[46–48] All the foldamers were prepared by the solid-phase method and purified by preparative reverse-phase HPLC (for details, see Supporting Information).

The folding propensities of these foldamers were examined by means of CD spectroscopy. The CD spectra in methanol are shown in Figure 5b. All foldamers displayed characteristic spectra of right-handed 12-helical β-peptides.[33–35] Foldamers **11–25** showed quite similar CD spectra, indicating that the overall populations of 12-helix were similar. The intensity at 222 nm is slightly diminished for **11–25** relative to **1**, suggesting that replacement of one cyclopentyl residue by an acyclic residue slightly decreased the stability of the 12-helix.

The inhibitory potency of foldamers **11–25** at 100 nM was measured by in vitro assay using recombinant substrate (Figure

dx.doi.org/10.1021/jm301306c | J. Med. Chem. 2013, 56, 1443–1454